© 2013. Published by The Company of Biologists Ltd | Development (2013) 140, 4544-4553 doi:10.1242/dev.098301

RESEARCH ARTICLE

Theoretical and experimental evidence indicates that there is no detectable auxin gradient in the angiosperm female gametophyte

Dmytro S. Lituiev[1], Nádia G. Krohn[2], Bruno Müller[1], David Jackson[3], Barbara Hellriegel[4], Thomas Dresselhaus[2] and Ueli Grossniklaus[1,*]

ABSTRACT

The plant life cycle alternates between a diploid sporophytic and a haploid gametophytic generation. The female gametophyte (FG) of flowering plants is typically formed through three syncytial mitoses, followed by cellularisation that forms seven cells belonging to four cell types. The specification of cell fates in the FG has been suggested to depend on positional information provided by an intrinsic auxin concentration gradient. The goal of this study was to develop mathematical models that explain the formation of this gradient in a syncytium. Two factors were proposed to contribute to the maintenance of the auxin gradient in *Arabidopsis* FGs: polar influx at early stages and localised auxin synthesis at later stages. However, no gradient could be generated using classical, one-dimensional theoretical models under these assumptions. Thus, we tested other hypotheses, including spatial confinement by the large central vacuole, background efflux and localised degradation, and investigated the robustness of cell specification under different parameters and assumptions. None of the models led to the generation of an auxin gradient that was steep enough to allow sufficiently robust patterning. This led us to re-examine the response to an auxin gradient in developing FGs using various auxin reporters, including a novel degron-based reporter system. In agreement with the predictions of our models, auxin responses were not detectable within the FG of *Arabidopsis* or maize, suggesting that the effects of manipulating auxin production and response on cell fate determination might be indirect.

KEY WORDS: *Arabidopsis*, Auxin, Female gametophyte, Gradient, Maize, Modelling

INTRODUCTION

The life cycle of plants alternates between a diploid sporophytic and a haploid gametophytic generation. In flowering plants, the sporophytic generation is the dominant form of the plant life cycle, whereas the gametophytic generation is highly reduced and short lived, and develops within the sexual organs of the flower.

In most flowering plants (70%), including *Arabidopsis thaliana* and *Zea mays* (maize), a postmeiotic female reproductive cell termed the functional megaspore (FM) undergoes three mitoses to form a female gametophyte (FG) comprising seven cells of four distinct cell types (Fig. 1).

[1]Institute of Plant Biology and Zürich-Basel Plant Science Center, University of Zürich, Zollikerstrasse 107, CH-8008 Zürich, Switzerland. [2]Cell Biology and Plant Biochemistry, Biochemie-Zentrum Regensburg, University of Regensburg, Universitätsstrasse 31, D-93053 Regensburg, Germany. [3]Cold Spring Harbor Laboratory, 1 Bungtown Road, Cold Spring Harbor, NY 11724, USA. [4]Anthropological Institute and Museum, University of Zürich, Winterthurerstrasse 190, CH-8057 Zürich, Switzerland.

*Author for correspondence (grossnik@botinst.uzh.ch)

Received 28 April 2013; Accepted 22 August 2013

In FG mutants with abnormally positioned or extra nuclei in maize (Evans, 2007; Srilunchang et al., 2010) and *Arabidopsis* (Gross-Hardt et al., 2007; Johnston et al., 2010; Moll et al., 2008; Pagnussat et al., 2007), the nuclei acquire their fate according to their spatial positioning along the micropylar-chalazal axis, suggesting that cell specification in the FG is driven by positional information. This hypothesis was strengthened by a microscopy study showing a graded activity of the auxin-sensitive reporter *DR5* (Ottenschläger et al., 2003) along the micropylar-chalazal axis of the FG (Pagnussat et al., 2009). Furthermore, overexpression of the auxin biosynthesis enzyme YUC1 and the artificial microRNA (amiRNA)-based knockdown of a group of auxin-dependent transcription factors (auxin response factors, ARFs) leads to the mis-specification of gametophytic cells (Pagnussat et al., 2009). Therefore, it was proposed that the phytohormone auxin is distributed in a gradient and serves as the morphogen driving cell specification in the *Arabidopsis* FG (Fig. 1) (Pagnussat et al., 2009; Sundaresan and Alandete-Saez, 2010).

Here, we attempted to reproduce the mechanisms of auxin gradient formation *in silico* for maize and *Arabidopsis* in order to verify whether the processes proposed previously, i.e. polar auxin influx at early stages and localised auxin synthesis at later stages (Pagnussat et al., 2009), are sufficient for the auxin gradient to be sustained, or whether additional factors should be considered. Using auxin degradation rates and diffusion coefficients from the literature, we found that only a very shallow auxin gradient can be maintained in *Arabidopsis* and a moderate one in maize, even if additional factors, such as background efflux or localised degradation, are incorporated into the model. Moreover, we showed that the steepness of the gradient obtained in our models does not allow a sufficiently robust cell fate acquisition, especially in the small *Arabidopsis* FG. Thus, we reanalysed the auxin response within ovules to refine our model. Surprisingly, we could not detect auxin-dependent *DR5* activity inside the FGs of either maize or *Arabidopsis* at any developmental stage. However, in both species we observed an auxin maximum in sporophytic nucellar cells at the micropylar pole of young ovules. As development progressed, *DR5* activity migrated towards the chalazal pole in the sporophytic tissues surrounding the FG. We propose a model involving non-cell-autonomous effects of auxin in the sporophytic tissues of the ovule, in which auxin overproduction in the FG can explain the cell fate changes observed by Pagnussat and colleagues (Pagnussat et al., 2009). Thus, auxin may affect cell specification indirectly through a function in sporophytic tissues rather than via a gradient in the FG.

RESULTS

Mathematical modelling shows that only shallow auxin gradients can be maintained in FGs

In order to elucidate potential mechanisms underlying the formation of an auxin gradient in angiosperm FGs, we developed a series of

Development (2013) doi:10.1242/dev.098301

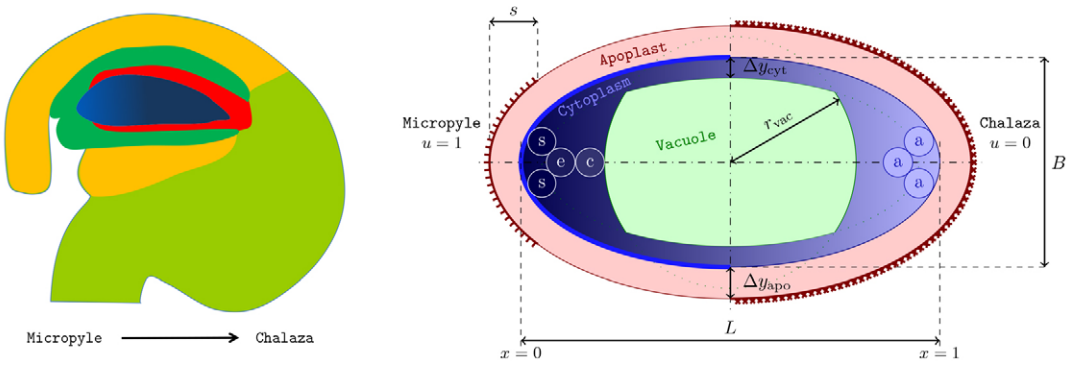

Fig. 1. Schematic representation of a FG. (Left) FG embedded in the context of the ovule. The endothelial tissue is shown in red, the inner integuments in green and the outer integuments in brown. (Right) Schematic of the FG showing features and geometrical parameters used in the simulations. An auxin gradient, which has been proposed to determine the cell fate of the synergids (s), egg cell (e), central cell (c) and antipodals (a), with decreasing concentration along the micropylar-chalazal axis is indicated in blue. The long axis of the FG from the micropylar (x=0) to the chalazal (x=1) pole is aligned with the x-axis in all models. The zone of auxin efflux is shown in dark-red pin lining. The zone where the concentration was set to zero is shown by dark-red x lining. The micropylar half of the plasma membrane where AUX1 was assumed to be expressed ≥5-fold higher than in the rest, is shown by a thick dark blue line. Not all proportions are preserved.

reaction-diffusion models based on the following assumptions: (1) auxin is produced or imported in the micropylar region of the FG; (2) auxin is degraded with first-order kinetics; and (3) diffusion of auxin is isotropic and homogenous throughout the cytoplasm.

We tested the contribution of different factor combinations (hereafter referred to as 'regimes') as described in Table 1. We included processes such as localised influx, both uniform and localised synthesis and degradation, as well as background efflux at the chalazal pole. As preliminary inspection showed that most parameter values produced only a very shallow gradient, we used parameter values that resulted in the steepest gradient, whenever alternative values were available from the literature (supplementary material Table S1).

PGP19 and AUX1 auxin carriers are expressed in the *Arabidopsis* FG

The distribution of auxin within plant tissues largely depends on polar auxin transport across membranes (reviewed by Garnett et al., 2010; Petrásek and Friml, 2009). Pagnussat and colleagues (Pagnussat et al., 2009) examined the expression of members of the PIN-FORMED (PIN) family of auxin transporters encoded by the *PIN1-4* and *PIN7* genes in the ovules and detected only PIN1 in the micropylar nucellar cells prior to the FG2 stage [all stages of FG development are given according to Christensen et al. (Christensen et al., 1997)]. Here, we further examined the expression of all other known auxin transporters in the FG. According to our RNA-Seq data, neither *PIN5* nor *PIN6* transcripts are detected in developing ovules (M. Schmid and U.G., unpublished). The PIN8 protein is not detected in ovules either (supplementary material Fig. S1), which is consistent with the fact that the *pin8-1* mutant is completely fertile (Dal Bosco et al., 2012).

In maize, we found ZmPIN1a-mRFP expression in sporophytic nucellar cells but not in the FG before the eight-nucleate stage (FG5), similar to previous findings in *Arabidopsis* (supplementary material Fig. S2; see also Fig. 7). In contrast to *Arabidopsis*, however, ZmPIN1a is expressed in the antipodal cells during FG maturation (stages FG6 and FG7). Because ZmPIN1a is expressed only at stages when the fate of the FG cells has already been determined, we did not consider this in our model.

The PGP1 (ABCB1) and PGP19 (ABCB19) efflux transporters are also known to participate in polar auxin transport (Geisler et al., 2005). Only PGP19 was found to be expressed in the *Arabidopsis* FG (supplementary material Figs S3, S4). The rates of PGP19-dependent and background auxin efflux used in our models were thus estimated based on earlier work by Geisler and colleagues (Geisler et al., 2005).

The AUXIN1/LIKE-AUX1 (AUX/LAX) family of transporters are known to facilitate auxin influx in *Arabidopsis* (Swarup and Péret, 2012). We found *AUX1* to be expressed in the *Arabidopsis* FG starting at the four-nucleate stage (FG4). Moreover, the protein accumulated in the micropylar part (supplementary material Fig. S5). Active auxin influx has been estimated to contribute up to 75% (Delbarre et al., 1996) of total auxin influx, with AUX1 contributing ~50% (Marchant et al., 1999), which was considered in our models. Close paralogs of *AUX1* with similar characteristics are either not detectable in the FG (*LAX3*) or are expressed at negligibly low levels (*LAX1* and *LAX2* at 2.2% and 1.0% of *AUX1* levels, respectively; M. Schmid and U.G., unpublished).

Table 1. Regimes used for the reaction-diffusion models

Parameter	Regime 1	Regime 2	Regime 3	Regime 4
Synthesis	None	Localised	None	None
Degradation	Uniform	Uniform	Localised	Uniform
Influx	Anterior pole	None	Anterior pole	Anterior pole
Efflux	None	None	None	Posterior pole

Measures of gradient steepness

As in most models of morphogen diffusion, our models were rescaled for analyses by combining the length of the FG, the diffusion coefficient, and the auxin degradation rate into a single parameter termed the characteristic length scale λ (Lander et al., 2009). However, as the models developed here account for boundary conditions relying on additional parameters, we could not use λ as a measure of the gradient steepness to compare different solutions. Therefore, we compared the different solutions based on a new measure termed the gradient steepness (GS), defined as the percentage by which the concentration drops towards the chalazal pole (u_{min}) from its maximum value (u_{max}) at the micropylar pole:

$$GS = \frac{u_{max} - u_{min}}{u_{max}} \cdot 100\% .$$

Development (2013) doi:10.1242/dev.098301

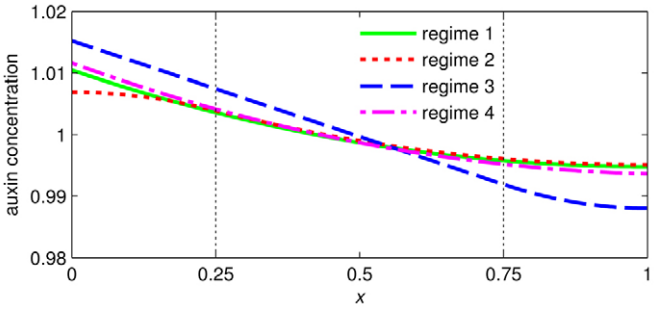

Fig. 2. Auxin concentration profiles in different regimes (one dimension) for *Arabidopsis*. The origin of the *x*-coordinate lies in the micropylar pole (*x*=0) and the axis runs towards the chalazal pole (*x*=1). Shaded areas represent the domains of localised synthesis (left) and degradation (right). Auxin concentration (*y*-coordinate) is presented in arbitrary units, assuming mean concentration = 1.

Simulation of the model in one dimension

Based on previous data indicating that the greatest variation in auxin concentration is observed along the micropylar-chalazal axis (Pagnussat et al., 2009), we studied a simplified one-dimensional model featuring spatial inhomogeneity of the processes along this axis. The spatial coordinate representing position along the micropylar-chalazal axis has its origin in the micropylar-most point (denoted as *x*=0) and spans the cytoplasm until the chalazal-most point (*x*=1) (Fig. 1). A numerical study of regime 1 (Table 1) in one dimension showed that the rate of auxin reaction-diffusion was much faster than the rate of FG growth, which allowed us to apply the quasi-steady state assumption with regard to reaction-diffusion (for details, see supplementary material Appendix S1). The absolute value of the error due to this simplification did not exceed 0.002% after 45 minutes of initial equilibration (supplementary material Fig. S6). Therefore, we focused on the eight-nucleate stage of FG development (FG5), when cell specification is believed to occur. At this stage, the FG of *Arabidopsis* reaches a length of up to 70 µm, whereas the maize FG is between 100 and 130 µm in the inbred line A188 (supplementary material Fig. S7).

The GS achieved under different regimes with parameter values obtained from the literature is shown in Fig. 2 and Table 2. Using regime 1 (localised influx and uniform degradation), a rather low GS of 0.78% was obtained for *Arabidopsis*; in maize, the GS reaches 2.66%. If we included local production of auxin at the micropylar pole instead of localised influx, as was suggested for late stages of FG development (Pagnussat et al., 2009), the simulation resulted in gradients that were even flatter than in the case of localised influx (Fig. 2, Table 2). By contrast, if we considered either localised degradation or background efflux of auxin, the steepness of the gradient increased (Figs 2, 4). Taken together, the simulations based on this one-dimensional model identified two factors capable of increasing GS compared with a result obtained with the simplest model (regime 1): background efflux producing a GS of 0.91% and 2.89% (regime 4) and localised degradation increasing the GS up to 1.36% and 4.55% (regime 3) in *Arabidopsis* and maize, respectively.

The large central vacuole can impede auxin diffusion in the FG, thereby increasing gradient steepness

At the two-nucleate stage (FG2), a large vacuole begins to form in the centre of the FG (Christensen et al., 1997; Schneitz et al., 1995; Huang and Sheridan, 1994). We investigated whether this vacuole can contribute to the maintenance of an auxin gradient in the FG by impeding the diffusion of auxin. To test this hypothesis, we set up a two-dimensional reaction-diffusion model with regimes 1 and 4, and solved it with the finite element method.

The results of this simulation showed that the large central vacuole will indeed impede diffusion, making the gradient steeper (Fig. 3, Table 2). This effect depends on the width of the cytoplasmic isthmus between the vacuolar and plasma membranes. Without the vacuole, two-dimensional models result in a GS that deviates less than 1% from that obtained with a one-dimensional model. However, with a width of the cytoplasmic isthmus of 1 µm, which is characteristic for *Arabidopsis* (supplementary material Fig. S8), the GS increases approximately two- to threefold in the two-dimensional model as compared with the model without a vacuole: from 1.33% to 3.21% in *Arabidopsis* and from 3.65% to 6.95% in maize (Fig. 4). In addition, taking localised AUX1-dependent influx into account, the GS decreases slightly by some thousandth of a percentage point (Fig. 4).

Thus, our simulations identify the effect of a vacuole together with carrier-dependent fluxes of auxin (by PGP19 and AUX1) as the most effective mechanisms that increase the steepness of a potential auxin gradient in the FG, leading to a GS of 3.21% and 6.95% in *Arabidopsis* and maize, respectively.

The theoretically achievable gradient of auxin cannot provide a sufficiently robust readout of positional information for cell specification

The morphogenetic signal providing positional information for cell specification can be corrupted by noise at different levels, both in its generation and perception (Lander et al., 2009). Perturbations of morphogen gradients can thus cause severe developmental aberrations and result in embryo lethality. Therefore, robustness is regarded as a major evolutionary constraint and is often used as an argument for or against the feasibility of theoretical models for morphogenetic gradients (e.g. Lander et al., 2009).

In order to theoretically assess the robustness of cell specification, we analysed the sensitivity of the theoretically achievable auxin gradient to perturbations in auxin concentration (for details see supplementary material Fig. S9 and Appendix S1). The auxin gradient obtained with physiological parameters is very shallow and makes the threshold position demarcating any two cell fate zones highly sensitive to perturbations in auxin concentration. A moderate perturbation of the auxin source by 3.5% leads to a positional shift of a given local auxin threshold throughout the entire length of the FG. Even a very small change of 0.5% in the auxin source leads to a shift of the threshold of at least 20%, which, for instance, is sufficient to disrupt cell specification in the micropylar part of the FG (Fig. 5; supplementary material Table S2). By contrast, a perturbation of the *Drosophila* Bicoid (Bcd)

Table 2. Gradient steepness (%) under different regimes

Species	Regime 1, 1D	Regime 2, 1D	Regime 3, 1D	Regime 4, 1D	Regime 4, 2D, evenly distributed AUX1, no vacuole	Regime 4, 2D, evenly distributed AUX1, with vacuole	Regime 4, 2D, polar AUX1, with vacuole
Arabidopsis	0.783	0.588	1.361	0.909	1.328	3.213	3.207
Maize	2.658	2.004	4.550	2.885	3.647	6.947	6.945

Development (2013) doi:10.1242/dev.098301

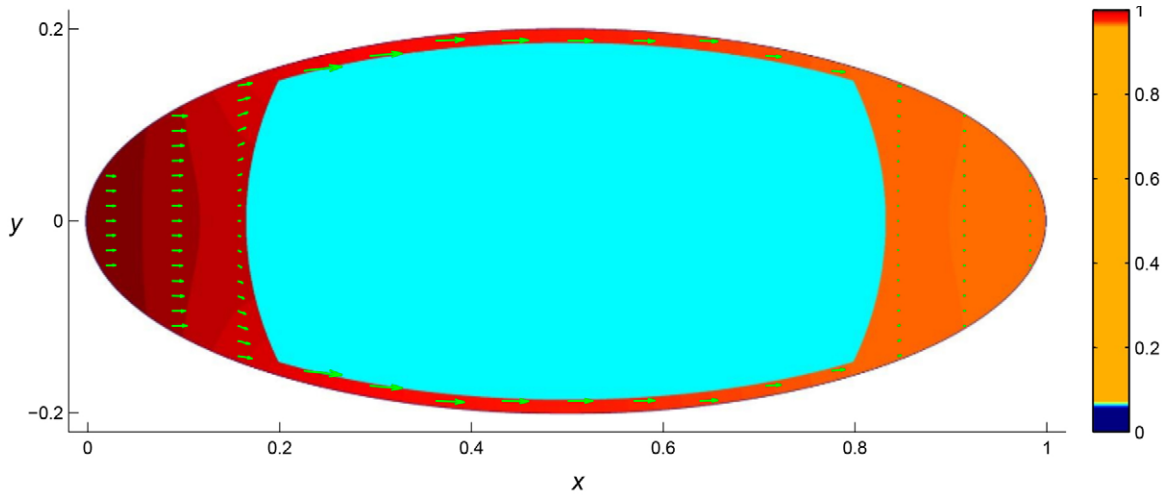

Fig. 3. Simulation result of the two-dimensional model in regime 4. Total auxin concentration is shown by colour code and auxin flux is indicated by green arrows (the length indicates flux intensity in logarithmic scale, arbitrary units). Note the maximal flux inside the cytoplasm is observed in the cytoplasmic isthmuses around the central vacuole. The colour code (right) is specially adjusted to emphasize the gradient.

gradient by 5% results in changes in the perceived position of less than 5% in the region where the positional information is read out under all parameters tested (de Lachapelle and Bergmann, 2010). Therefore, the theoretical auxin gradient in the FG is extremely sensitive to perturbations compared with the well-studied *Drosophila* Bcd gradient and is thus highly unlikely to provide the stable positional information required for cell specification.

In summary, the auxin gradient obtained with known, realistic parameters is very sensitive to variation in the auxin source and thus would make cell specification highly unreliable. This result can be interpreted as follows: (1) the rate of auxin diffusion or background efflux in the FG is drastically different from that in all other known cases, which is very unlikely; (2) additional factors, for instance efflux mediated by as yet unknown transporters, contribute to the maintenance of the gradient; or (3) the auxin gradient achieved under these realistic conditions is not sufficient, or provides only part of the positional information needed, for cell fate determination; for instance, auxin might be a trigger of polarisation but not provide the positional information required for cell specification.

Microscopy analyses of auxin activity in *Arabidopsis* and maize ovules reveal no auxin activity inside the FG

Our modelling results predicted only very shallow auxin gradients using known, realistic parameters in *Arabidopsis* and, to a lesser extent, in maize. To test this prediction, we aimed to characterise auxin activity in the ovule and FG experimentally in both *Arabidopsis* and maize using the classical *DR5* auxin-sensitive promoter (Ulmasov et al., 1997) and novel reporters based on auxin-dependent protein degradation.

Auxin response in ovules of *Arabidopsis thaliana*

Three different *DR5* lines were studied, each harbouring a different fluorescent protein: an endoplasmic reticulum (ER)-targeted GFP (Ottenschläger et al., 2003), a nuclear-targeted triple GFP (Weijers et al., 2006), and a nuclear localised tandem Tomato (tdTomato) fluorescent protein; the latter line additionally carried a nuclear YFP expressed under the gametophyte-specific *AKV* promoter (Rotman et al., 2005), marking all gametophytic nuclei. All three lines displayed the same pattern of *DR5* activity. At the megaspore mother cell (MMC) stage (Fig. 6A,F,K), *DR5* activity was observed in cells of the L1 and sometimes L2 layer of the nucellus surrounding the MMC, mostly at the future micropylar pole. Later, at the FM stage (FG1, Fig. 6B,G,L), the highest *DR5* activity was observed in the micropylar region of the nucellus in cells of the L1 and L2 layer, with some activity in the L2 cells surrounding the FM laterally. At the early two-nucleate stage of FG development (FG2, Fig. 6C,H,M), the pattern remained largely the same; however, the FG begins to displace the nucellar tissue (Schneitz et al., 1995) and, in the late two-nucleate stage (FG3, Fig. 6D,I,N), at its micropylar pole the FG comes into contact with the inner integuments, which lack *DR5* expression. At the four-nucleate stage (FG4, Fig. 6E,J,O), most of the nucellar tissue

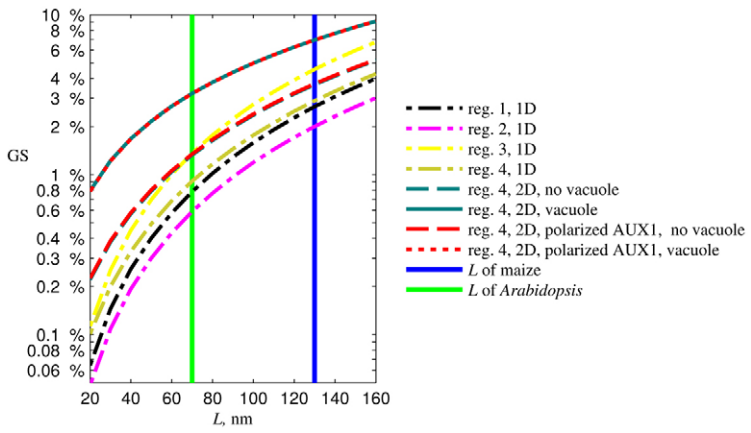

Fig. 4. Dependence of the gradient steepness on the length *L* of the FG for different model modifications. Localised synthesis (regime 2) is assumed to occur in the 1/4 micropylar-most part, whereas localised degradation (regime 3) is assumed to occur in the 1/4 chalazal-most part of the FG. The FG sizes (*L*) for *Arabidopsis* and maize at stage FG5 are indicated by vertical lines. Regime 4 in two dimensions results in maximal gradient steepness, especially when a vacuole is included. Addition of AUX1 to the model in regime 4 (2 dimensions) results in only a very minor increase in the gradient steepness. In maize, due to the larger size of the FG, steeper gradients can be achieved.

Development (2013) doi:10.1242/dev.098301

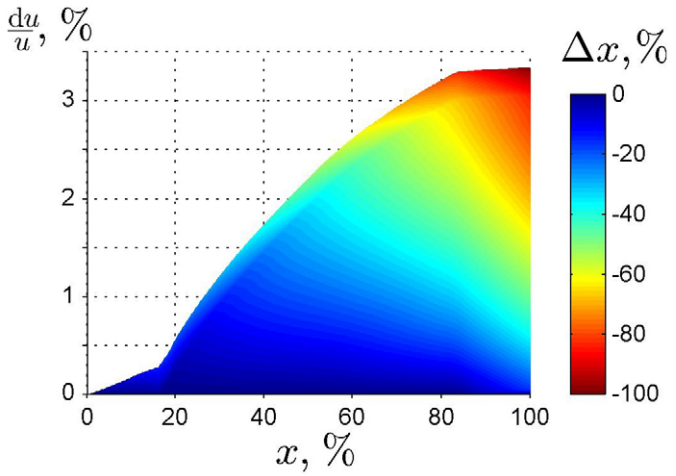

Fig. 5. The theoretically achievable auxin gradient is highly sensitive to noise in the auxin concentration. The value of the predicted positional variability of the threshold position as a response to a perturbation in the auxin concentration (equivalent to a shift in source intensity) in percentage of the length of the FG is indicated in colour code. The blank space represents the positions where the perturbation shifts the perceived threshold position out of the domain boundaries (i.e. no cells in the FG can achieve the cell fate determined left of the corresponding threshold position anymore). Note that a perturbation of ~0.51% disrupts cell specification in the micropylar part of the FG (x<0.2) and any perturbation higher than 3.5% disrupts it in the entire FG.

in the micropylar and medial part has degenerated and *DR5* activity is concentrated in the nucellar tissue adjacent to the chalazal pole of the FG. Later, at the final developmental stages (FG5 and FG6), some sporophytic cells adjacent to the chalazal pole of the FG were found to express *DR5* (supplementary material Fig. S10). From the four-nucleate until the final stages, a single *DR5*-expressing cell can be seen at the micropylar tip of the inner integument in fewer than a quarter of the ovules.

To obtain an alternative auxin signalling readout, we developed transgenic plants carrying a novel degron-GFP sensor, which exploits the auxin-dependent degradation of AUX/IAA proteins. Auxin binding to the ubiquitin ligase TRANSPORT INHIBITOR RESPONSE1 (TIR1) causes the degradation of AUX/IAA proteins via their domain II (Ramos et al., 2001). We used the six amino acid domain II core VGWPPV peptide, which is common to more than 70% of AUX/IAA isoforms (Ramos et al., 2001), as a C-terminal fusion to GFP6. An analogous reporter, DII-Venus, was developed in parallel (Vernoux et al., 2011) but is driven by the *35S* promoter, which is thought to be inactive in the FG (Desfeux et al., 2000) (U.G., unpublished) and was not detected in the FG (supplementary material Fig. S11). By contrast, a bright signal of degron-GFP driven by the ubiquitin 10 (*UBQ10*) promoter (*pUBQ10*) is visible throughout FG development (Fig. 6P-T), indicating that there is not a sufficiently high auxin concentration to cause degradation of the reporter. Although degron-GFP levels during the initial stages of ovule development are lower in sporophytic tissues than in the developing FG, an even lower level was detected in nucellar cells that express *DR5* (Fig. 6P,Q). Thus, the pattern of auxin activity inferred from degron-GFP is complementary to the pattern displayed by the *DR5* promoter. Thus, even though the dynamic range of degron-GFP activity apparently lies in a lower range of concentrations than that of *DR5*-driven fluorescent proteins, the qualitative patterns displayed by both are consistent.

We observed lower levels of degron-GFP in many sporophytic cells than in the FG, even though neither displayed *DR5* activity. This prompted us to test whether *pUBQ10* showed differential activity in these cells and to use a control pUBQ10::GFP line to estimate relative auxin levels. A comparison of fluorescence intensities between pUBQ10::degron-GFP and control pUBQ10::GFP lines allowed us to correct for inhomogeneities in the protein levels due to differences in promoter activity. Accounting for these corrections, degradation of degron-GFP is significantly higher in the nucellar cells surrounding the FG than in the FG at both the FM (FG1) and late two-nucleate (FG3) stages (supplementary material Fig. S12, Table S3), which is in agreement with the pattern displayed by the *DR5* promoter.

In conclusion, we could not detect any auxin activity inside the *Arabidopsis* FG experimentally. On the contrary, we found that until the late two-nucleate stage (FG3) the ovule's minimum auxin activity is localised in the FG. Moreover, the pattern of auxin activity in the sporophytic nucellus tissue is highly dynamic and exhibits the following features: (1) an auxin maximum usually in the two epidermal cells (L1 layer) at the tip of the ovule as the MMC differentiates in the L2 layer; (2) migration of the *DR5* activity maximum from the micropylar towards the chalazal pole; and (3) degeneration of *DR5*-expressing cells in the micropylar region of the nucellus.

Auxin response in ovules of *Zea mays*

In maize, we studied the expression pattern of *DR5* driving an ER-targeted red fluorescent protein (mRFP:ER) (Gallavotti et al., 2008). As shown in Fig. 7A, a strong *DR5* signal was visible at the tip of an ovule primordium in a few epidermal cells of the L1 layer in immediate proximity to a subepidermal cell of the L2 layer that differentiates into the MMC. The auxin response expanded around this cell, which enlarges at its micropylar pole and elongates longitudinally, and which appears smaller towards its chalazal pole (Fig. 7B,C). The nucleus of the emerging, highly polarised MMC moved towards the micropylar pole close to the auxin maximum, and initiated meiosis. After completion of meiosis, the three micropylar-most megaspores degenerated and the FM (FG1) became more deeply embedded into the L3 layer of the developing ovule (Fig. 7D-F).

Although the cells showing *DR5* activity at the tip of the ovule expanded to the L2 layer, these sporophytic auxin-responsive cells were no longer neighbouring the FG after the FG1 stage. During FG development, *DR5* activity decreased, beginning at stage FG2 (Fig. 7G-I), and was no longer detectable in micropylar nucellar cells from stage FG5 onwards (Fig. 7J). In mature ovules, *DR5* activity was entirely absent from this region at stage FG7 (Fig. 7K,L; supplementary material Fig. S13). By contrast, a strong *DR5* signal became visible in the tips of the inner and outer integuments (Fig. 7J; supplementary material Fig. S13A,B), as well in the gametophytic antipodal cells, with the strongest signals in the antipodal cells located furthest from the central cell (Fig. 7K,L; supplementary material Fig. S13C,D).

In conclusion, *DR5* activity, and thus a nuclear auxin response gradient, was not observed inside the developing FG of maize before the completion of cellularisation at stage FG6, by which time cell specification has presumably already taken place. The only gametophytic *DR5* signal was observed in the antipodal cells, after cellularisation and during their proliferation.

Sporophytic non-cell-autonomous effects may explain cell fate changes in the FG

Our theoretical results suggested that, with known parameters, an auxin gradient cannot be maintained in the FG, and our experimental

Development (2013) doi:10.1242/dev.098301

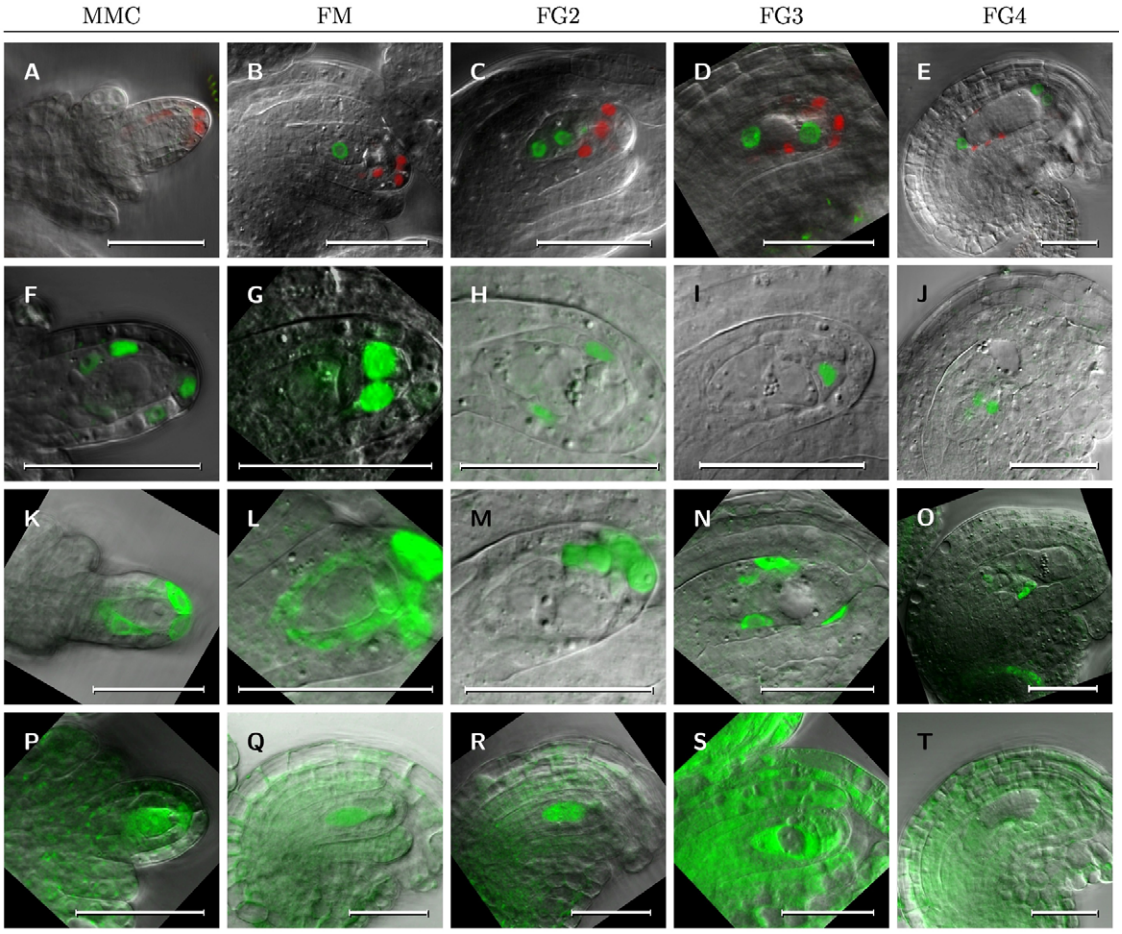

Fig. 6. Auxin response in *Arabidopsis* ovules during FG development. Stages of ovule development using four independent auxin reporter lines (see text for details). The following stages are shown: megaspore mother cell (MMC), functional megaspore (FM, also referred to as FG1), two-nucleate FG (FG2), two-nucleate FG with large central vacuole (FG3) and four-nucleate FG (FG4). (A-E) DR5::Dof1a:tdTomato (red) line with the AKV::H2B:YFP gametophytic fate marker (green); (F-J) DR5::SV40:3×GFP; (K-O) DR5::GFP-ER; (P-T) pUBQ10::degron-GFP. The images are oriented such that the micropylar pole of the ovules points to the right. At the MMC (A,F,K,P), FM (B,G,L,Q) and FG2 (C,H,M,R) stages auxin activity is observed only in cells surrounding the MMC or FG. At early stages, the maximum auxin activity is in the epidermal cells at the very micropylar tip of the ovule; later, also sporophytic cells in lateral regions of the nucellus show high auxin activity. At the FG2 stage (D,I,N,S) the nucellar tissue surrounding the FG begins to degenerate, starting at the micropylar pole. Some lateral sporophytic cells show auxin activity. At the FG4 stage (E,J,O,T) the surrounding nucellar tissue continues to degenerate; cells with a maximum in auxin activity are found more towards the chalazal pole. Throughout its development, no auxin activity can be observed within the FG (note that there is no overlap of the green gametophytic cell fate marker with the red DR5-driven fluorescent protein in the top row). Scale bars: 30 μm.

data showed that indeed no auxin activity can be detected inside the FGs of *Arabidopsis* and maize. However, earlier experiments had shown that auxin overproduction in the *Arabidopsis* FG can lead to changes in the fate of gametophytic nuclei (Pagnussat et al., 2009). Based on the results presented here, this change in cell fate does not come about by altering the auxin gradient inside the FG as previously interpreted. Here, we suggest an alternative hypothesis that can explain such changes through effects of auxin overproduction in the FG on the surrounding sporophytic tissues. Given that there is no detectable auxin gradient in the FG but that (1) there is polarised auxin activity in the sporophyte and (2) there are effects of auxin overproduction on gametophytic cell specification, it is likely that auxin has some effect in sporophytic tissues that indirectly affects cell fate decisions in the FG, namely via a non-cell-autonomous signal (NCAS).

To examine whether such a scenario could explain the experimental observations made by Pagnussat and colleagues (Pagnussat et al., 2009), we used as a basis the two-dimensional steady state model with a vacuole described above. We developed a mathematical model that is based on the assumption that the promoter of NCAS is responsive to auxin in sporophytic cells. Auxin leads to its activation in an all-or-none manner, i.e. the promoter becomes active if the concentration of auxin exceeds a certain threshold concentration c_{thr}. This serves as a good approximation for a more realistic scenario using a Hill activation function (e.g. Alon, 2007). The NCAS diffuses throughout the domain and is degraded inside the cells with the rate a_{NCAS}. For simplicity, we assumed that its diffusion coefficient in the membrane has the same value as in the cytoplasm (D_{NCAS}) (see supplementary material Table S4 for the values of parameters used).

Using this model, we studied the impact of auxin overproduction inside the FG on the spatial distribution of the NCAS. The concentration of auxin, the activity of the NCAS promoter, and the concentration of NCAS itself are visualised in Fig. 8 under different levels of auxin synthesis. It is obvious that, depending on the level of auxin production in the FG (and the promoter activation threshold; data not shown), different spatial distributions of the NCAS can be achieved. In fact, high levels of auxin production lead

Development (2013) doi:10.1242/dev.098301

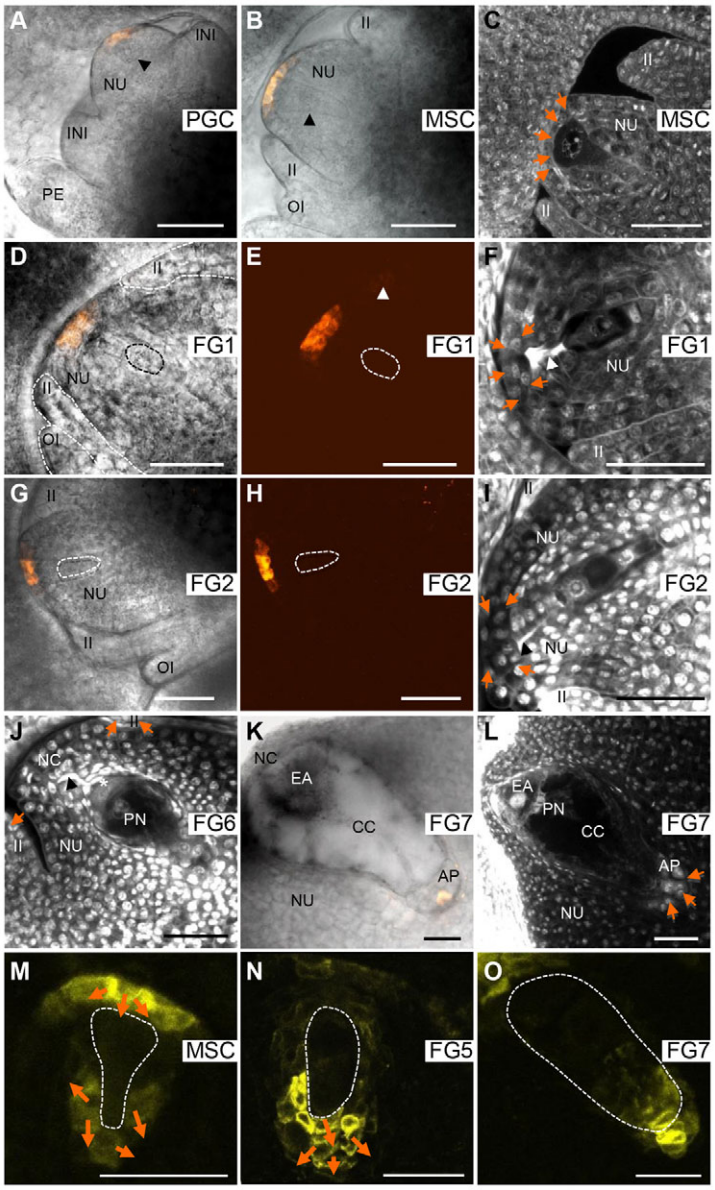

Fig. 7. Auxin response and flux in the maize ovule during female germline development. DR5::mRFP:ER (A-L) and ZmPIN1a::PIN1a:YFP (M-O). Developmental stages are indicated in each panel. (A) A subepidermal L2 nucellar cell in immediate proximity to strongest *DR5* reporter expression in L1 differentiates into the primordial germ cell (PGC; arrowhead). (B) The PMC has differentiated into a highly polar MMC (arrowhead). (C) Section through the ovule at MMC stage. MMC is in pachytene stage of meiosis I. Arrows point towards a single L1 nucellus cell layer displaying a strong auxin response in B. (D,E) *DR5* expression after meiosis at stage FG1. Three megaspores degrade and the FM is encircled. *DR5* activity expands to the L2 micropylar nucellus. Arrowhead in E indicates the L1 layer. (F) Section through the ovule at stage FG1. Remnants of degenerated megaspores are indicated by an arrowhead. Arrows point towards L1 and L2 nucellar cells showing a strong auxin response in fluorescent images. (G,H) Stage FG2. The FG is indicated by the white dashed line. (I) Ovule at stage FG2. Remnants of degenerated megaspores are indicated by an arrowhead and nucellar cells showing an auxin response in fluorescent images are indicated by arrows. (J) Ovule at stage FG6. Cellularisation of the FG has completed. The egg cell nucleus is located below the asterisk. Arrowhead indicates remnants of degenerated megaspores and arrows indicate an auxin response in integument tips of fluorescent images. (K) Mature FG containing more than 20 antipodal cells. Integuments were removed. (L) Section through the ovule at mature stage FG7. Antipodal cells showing an auxin response are indicated by arrows. (M) Auxin flux in L1 micropylar nucellar cells points towards the highly polar MMC (outlined by dashed line), but is depleted at its chalazal pole. (N) At stage FG5, ZmPIN1a is visible at high levels in nucellar cells surrounding the chalazal pole of the FG. (O) At stage FG6 ZmPIN1a is expressed inside antipodal cells. (A,B,D,K) Merged brightfield und epifluorescent images. (E,H) Fluorescence images of D and G, respectively. (C,F,I,J,L) Stack of confocal sections of fixed ovules. (M-O) Fluorescent images of ZmPIN1a-expressing ovules. Orange arrows indicate the cells showing a strong auxin response, as shown by DR5 expression. AP, antipodal cells; CC, central cell; EA, egg apparatus; II, inner integument; INI, integument initials; NC, nucellar cap; NU, nucellus; OI, outer integument; PE, pericarp; PN, polar nuclei. Scale bars: 50 μm.

to a complete loss of polarity in the spatial distribution of NCAS (Fig. 8), which is expected to result in cell fate changes.

In summary, the changes in nuclear fate observed upon auxin overproduction inside the FG can be explained by auxin flux into the surrounding sporophytic tissues. This will lead to an expansion of the auxin response beyond the area seen in wild-type ovules at the chalazal pole and may have indirect effects on cell specification inside the FG.

DISCUSSION

Our modelling results show that even under the most beneficial parameters and assumptions, the concentration of auxin drops from one end of the FG to the other only by 3.2% and 6.9% in *Arabidopsis* and maize, respectively. This is much lower than, for instance, the steepness of the Bcd gradient in *Drosophila*, which is more than 90% (Gregor et al., 2005; He et al., 2010). We found that such a shallow gradient is highly sensitive to perturbations in the auxin source, and perturbations of 3.5% or more in the auxin source completely disrupted patterning in the FG, whereas for the Bcd gradient such perturbations would lead to a shift of the threshold position of merely 4%. Therefore, such a shallow gradient would compromise the robustness of cell specification with regard to the various fluctuations that are inherent to biological systems, especially in the intensity of the auxin source. We conclude that the factors studied do not allow the production of a sufficiently steep auxin gradient to provide enough positional information for cell specification in the FG. This led us to an attempt to quantify *DR5* activity in the FG in order to refine the model.

Unexpectedly, our microscopy studies showed that, in contrast to a previous report (Pagnussat et al., 2009), auxin-dependent activity cannot be detected inside developing FGs in *Arabidopsis* or maize. Additionally, we found that the pattern of auxin activity in sporophytic cells adjacent to the FG is highly dynamic. The most notable developmental change in the pattern of auxin activity in the *Arabidopsis* ovule is the progressive movement of auxin maxima in cells adjacent to the developing FG from the micropylar towards the chalazal pole. It is tempting to speculate that this polarised activity could trigger indirect, non-cell-autonomous effects that influence cell specification inside the FG. Similarly, in maize, auxin activity was not observed inside the FG until cellularisation was complete.

Development (2013) doi:10.1242/dev.098301

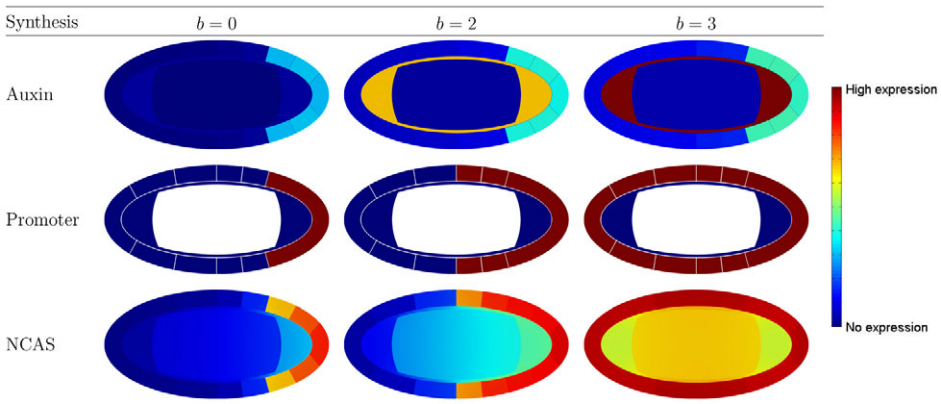

Fig. 8. Overproduction of auxin in the FG can lead to expansion of a auxin-induced non-cell-autonomous signal in the sporophyte and loss of polarity. Expression of auxin is shown in a heat map colour code. The FG is oriented such that the micropylar pole is on the left. Different levels of auxin expression (*b*=0, 2, 3) are represented in the three columns: the first column represents a situation when no auxin is synthesized in the FG, whereas the following two columns show increasing levels of auxin expression inside the FG, which ultimately leads to a loss of polarity in the sporophytic tissues surrounding the FG. See text for details.

Instead, auxin activity was detected in adjacent sporophytic nucellar cells of the micropylar pole at early stages and in proliferating antipodal cells during FG maturation. A similar pattern has recently been described in *Hieracium pilosella*, in which no evidence for *DR5* activity inside the FG was found (Tucker et al., 2012).

Taken together, our theoretical and experimental studies are inconsistent with the earlier report of a graded auxin-dependent activity in the FG of *Arabidopsis* (Pagnussat et al., 2009). This gives us reason to believe that these earlier results were misinterpreted and that the area with *DR5* activity assigned to the FG in fact encompassed a larger area including sporophytic cells in the nucellus, which indeed express DR5::GFP-ER. The exact boundary of the FG might not be easily identifiable by epifluorescence microscopy, as used in the previous study (Pagnussat et al., 2009), but is very clear under a confocal laser-scanning microscope and, especially, with nuclear localised reporters (Fig. 6A-J).

However, the experimental manipulations of auxin synthesis (by *YUC1* overexpression) and signalling (amiRNA-mediated knockdown of ARFs) in the FG that perturbed gametophytic cell fate seemed consistent with the hypothesis of an auxin gradient (Pagnussat et al., 2009) and warrant an explanation. Here, we propose hypotheses that are consistent with the effects on cell specification observed in these studies. First, changes in the fate of gametophytic nuclei can be explained by sporophytic effects of auxin overproduction in the FG. Using a modelling approach, we showed that auxin overproduction can indeed lead to a breakdown of polarity and loss of positional information inside the FG that results from auxin leakage into sporophytic tissues. In fact, our theoretical results agree with previous observations that showed an expansion of *DR5* activity into the surrounding sporophytic tissues upon *YUC1* overexpression [figure S5 in Pagnussat et al. (Pagnussat et al., 2009)]. Such an effect would be mediated by a hypothetical auxin-dependent NCAS, which is produced in sporophytic cells and controls cell specification in the FG. For instance, the peptide ZmEAL1 secreted from the egg cell has recently been shown to regulate cell fate within the maize FG in a non-cell-autonomous manner (Krohn et al., 2012). Similarly, peptides controlling cell fate in the FG could be secreted by surrounding nucellar cells.

Second, the effects observed by Pagnussat and colleagues (Pagnussat et al., 2009) could be mediated by some auxin-independent components of auxin signalling in the FG. For example, the transcription factors ARF3 and ARF17 possess auxin-like activity but are uncoupled from auxin signalling (Guilfoyle and Hagen, 2007). Both are transcribed in the central cell (Schmid et al., 2012) and show polarised mRNA expression in FGs at the four-nucleate stage (M. Schmid and U.G., unpublished). Downregulation of one of these factors, such as ARF3 in the experiment described by Pagnussat and colleagues (Pagnussat et al., 2009), would reduce such an auxin-independent auxin-like signal, whereas auxin overproduction would mask effects of ARF3 and/or ARF17 expression. Nevertheless, the activity of ARF3 or ARF17 should theoretically be detectable by the *DR5* sensor; the fact that *DR5* activity is not observed in the FG could mean that this activity is below the threshold of detection.

Finally, there could be minimal auxin-dependent activity in the FG that is below the detection level of any of our reporter systems with a very shallow gradient. Even though our modelling has shown that this gradient cannot provide positional information that is sufficiently robust for cell specification, it could determine the polarity of another morphogen through so-called wave-pinning (Mori et al., 2008). Such a model depends on two interconverting molecular species, whereby a progressing but eventually decelerating activation wave of one species would be initiated at one pole of the FG, leading to the depletion of the second species in this process. Thus, wave pinning could convert a spatially more or less homogeneous concentration profile into an asymmetric stationary front profile. However, wave pinning crucially depends on very different rates of diffusion of the two species, with the active form having the low diffusion rate. For instance, the interconversion of membrane-bound and a soluble forms of Rho GTPases can polarize cells by wave-pinning (Mori et al., 2008). Auxin is known to activate the ROP2 and ROP6 Rho GTPases in *Arabidopsis* epidermal cells through a yet poorly understood transcription-independent auxin signalling pathway (Xu et al., 2010). However, it is unknown whether Rho GTPases play a role in FG development or whether any other signaling molecules in the FG fulfil the requirements for wave pinning, i.e. rapid interconversion and highly different diffusion rates.

Although alternative explanations for the outcome of the experiments perturbing auxin production and signalling can be provided, there are currently not enough data to suggest a more precise mechanism. In particular, the most frequent cell fate change observed in both auxin overproduction and ARF amiRNA knockdown experiments was a loss of cell fate marker expression, whereas misexpression of egg and synergid cell markers was rather rare (Pagnussat et al., 2009). Thus, additional experiments that allow a more precise manipulation of auxin and/or other factors within and outside the FG will be required to develop accurate models of cell specification in the FG. In conclusion, neither our theoretical nor experimental evidence supports the hypothesis that a gradient in auxin activity provides the positional information for cell specification in the FG of flowering plants.

MATERIALS AND METHODS

Mathematical simulations

One-dimensional solutions were found analytically and were simulated in MATLAB 2011b software (MathWorks, Natick, MA, USA) using the *pdepe* function. Two-dimensional simulations were carried out with COMSOL Multiphysics 4.3a software (COMSOL Group, Stockholm, Sweden), exploiting the finite element method. To study the robustness of patterning, one-dimensional data or one-dimensional averages of two-dimensional simulations were used. Details are provided in supplementary material Appendix S1 and Tables S1, S4 and S5.

Generation of transgenic constructs

The DR5::NLS:tdTomato plasmid was constructed using a 35Smin:TMVΩ:Dof1a:tdTomato vector (B.M., unpublished), which is derived from a pCB302 binary vector (Xiang et al., 1999), carrying the TMVΩ translational enhancer (Gallie, 2002) and the Dof1a nuclear localisation signal (NLS) (Yanagisawa and Sheen, 1998) translationally fused to the tdTomato fluorescent protein gene (Shaner et al., 2004). The PCR-amplified *DR5* synthetic promoter from the DR5::GFP-ER plasmid (Ottenschläger et al., 2003) was inserted into the Ω:Dof1a:tdTomato vector.

The pUBQ10::degron:GFP plasmid was obtained by inserting a sequence encoding the degron consensus core of AUX/IAA proteins (VGWPPV) into the pMDC111 vector (Curtis and Grossniklaus, 2003) with subsequent Gateway insertion of the 2.5 kb *Arabidopsis* ubiquitin *UBQ10* promoter as explained in supplementary material Fig. S14. The control pUBQ10::GFP construct was obtained similarly. The constructs were verified by sequencing.

Plant material and growth conditions

The *Arabidopsis* DR5::GFP:ER line (Ottenschläger et al., 2003) was obtained from Jiří Friml (Flanders Institute of Biotechnology, Belgium), DR5::SV40:3×GFP (Weijers et al., 2006) from Dolf Weijers (Wageningen University, The Netherlands), and the DR5::NLS:tdTomato line is described here for the first time (see above). The PGP1::PGP1:GFP line in a *pgp1* homozygous background, the PGP19::PGP19:GFP line in a *pgp19* homozygous background (Geisler et al., 2005), and the AUX1::AUX1:YFP line in a *aux1-22* homozygous background (Swarup et al.,. 2004) were provided by Markus Geisler (Université de Fribourg, Switzerland); the PIN8::PIN8:GFP line (Dal Bosco et al., 2012) was provided by Cristina Dal Bosco (Albert-Ludwigs-Universität Freiburg, Germany). Unless indicated otherwise, all plants used were *Arabidopsis thaliana* (L.) Heynh. var. Columbia-0 (Col-0).

DR5::NLS:tdTomato transformants were obtained by *Agrobacterium*-mediated floral dip transformation (Bent, 2006). Seven independent transformants were recovered from BASTA selection and microscopically screened for tdTomato expression in ovules in the T1 (heterozygous plants) and T3 (homozygous plants) generations; a qualitative variation in expression patterns among the seven independent lines was not observed. A representative DR5::NLS:tdTomato line was crossed with the AKV::H2B:YFP gametophytic fate marker line (Rotman et al., 2005), provided by Wei-Cai Yang (Chinese Academy of Science, Beijing, China), which is in the Landsberg (*erecta* mutant, L*er*) background, and F3 plants homozygous for both constructs were analysed.

Arabidopsis plants were grown as described (Schmid et al., 2012). For DR5::SV40:3×GFP seeds, the plates were supplemented with kanamycin (AppliChem, Darmstadt, Germany) to a final concentration of 50 µg/ml. Glufosinate (Plüss-Staufer, Oftringen, Switzerland) was sprayed onto plants carrying the DR5::NLS:tdTomato transgene on the third and sixth day after transfer to soil at a final concentration of 0.2 g/l.

Maize inbred lines A188 and H99 and transgenic lines (Gallavotti et al., 2008) were grown under standard greenhouse conditions at 26°C with 16 hours of light and a relative air humidity of ~60%.

Microscopy and image acquisition

Ovules of *Arabidopsis* plants at various stages were dissected and studied either cleared for 5-15 minutes with 1 M glycine (pH 9.6) solution (as in Fig. 6H-J,M,O) or untreated in water (all other images). The pictures were taken with a Leica SP2 laser-scanning confocal microscope (Leica Microsystems AG, Heerbrugg, Switzerland). The GFP fluorescence was collected at wavelengths of 501-532 nm. For simultaneous YFP and tdTomato imaging, scanning was performed sequentially. Emission light of 503-575 nm and 575-632 nm was collected for the yellow and red channels, respectively. An excitation beam splitter DD 488/543 was used in both cases. Image capture was performed using Leica Confocal Software 2.61 and channel overlay was performed using a custom MATLAB script.

Maize cobs were harvested from greenhouse-grown plants. Whole cobs were treated as described (Srilunchang et al., 2010). For microscopy analyses, ovaries were dissected after clearing, mounted in methyl salicylate, and analysed with an LSM 510-META confocal laser-scanning microscope (Carl Zeiss Microscopy GmbH, Oberkochen, Germany) with 488 nm excitation and a LP 505 filter. For selective ZmPIN1a::PIN1a:YFP visualisation, 514 nm excitation and a BP 530-600 filter were applied, whereas DR5::mRFP:ER fluorescence was observed with 543 nm excitation in combination with a BP 560-615 filter. Image capture and processing were performed using the Zeiss LSM 510 META software and Zeiss LSM Image Browser version 3.5.0.359.

Note added in proof

While our manuscript was under revision, Ceccatto and colleages (Ceccatto et al., 2013) also reported the absence of DR5 activity in the *Arabidopsis* FG.

Acknowledgements

We thank Dolf Weijers (Wageningen University), Jiří Friml (Flanders Institute of Biotechnology), Wei-Cai Yang (Chinese Academy of Science), Markus Geisler (Université de Fribourg) and Cristina Dal Bosco (Albert-Ludwigs-Universität Freiburg) for seeds; Célia Baroux and Christof Eichenberger (University of Zürich) for advice on confocal microscopy; Marc Schmid (University of Zürich) for allowing us to cite unpublished data; Pierre Barbier de Reuille (University of Berne), Enrico Martinoia (University of Zürich), Leah Edelstein-Keshet (University of British Columbia) and Markus Geisler for discussion; and Lucia Colombo (Universita degli Studi di Milano) for critical comments on the manuscript.

Competing interests

The authors declare no competing financial interests

Author contributions

D.S.L. developed and simulated the mathematical models; D.S.L. and N.G.K. conducted experimental studies in *Arabidopsis* and maize, respectively; B.M. and D.J. provided materials; B.H. provided expertise for modeling; T.D. initiated and supervised the maize experiments; U.G. conceived and supervised the project; D.S.L. and U.G. wrote the manuscript, with input from all authors.

Funding

This work was supported by the Universities of Zürich and Regensburg, a postgraduate scholarship (Coordenação de Aperfeiçoamento de Pessoal de Nível Superior-CAPES-Brasília/Brazil) to N.G.K, and an iPhD Project of SystemsX.ch, the Swiss Initiative in Systems Biology to U.G., B.H. and B.M.

Supplementary material

Supplementary material available online at
http://dev.biologists.org/lookup/suppl/doi:10.1242/dev.098301/-/DC1

References

Alon, U. (2007). *An Introduction to Systems Biology: Design Principles of Biological Circuits*, pp. 15. Boca Raton, FL: Chapman & Hall/CRC.

Bent, A. (2006). Arabidopsis thaliana floral dip transformation method. *Methods Mol. Biol.* **343**, 87-103.

Chavarría-Krauser, A. and Ptashnyk, M. (2010). Homogenization of long-range auxin transport in plant tissues. *Nonlinear Anal. Real World Appl.* **11**, 4524-4532.

Christensen, C. A., King, E. J., Jordan, J. R. and Drews, G. N. (1997). Megagametogenesis in Arabidopsis wild type and the Gf mutant. *Sex. Plant Reprod.* **10**, 49-64.

Ceccato, L., Masiero, S., Sinha Roy, D., Bencivenga, S., Roig-Villanova, I., Ditengou, F.A., Palme, K., Simon, R., and Colombo, L. (2013). Maternal control of PIN1 is required for female gametophyte development in Arabidopsis. *PLoS ONE* **8**, e66148.

Curtis, M. D. and Grossniklaus, U. (2003). A gateway cloning vector set for high-throughput functional analysis of genes *in planta*. *Plant Physiol.* **133**, 462-469.

Dal Bosco, C., Dovzhenko, A., Liu, X., Woerner, N., Rensch, T., Eismann, M., Eimer, S., Hegermann, J., Paponov, I. A., Ruperti, B. et al. (2012). The

endoplasmic reticulum localized PIN8 is a pollen specific auxin carrier involved in intracellular auxin homeostasis. *Plant J.* **71**, 860-870.
de Lachapelle, A. M. and Bergmann, S. (2010). Precision and scaling in morphogen gradient read-out. *Mol. Systems Biol.* **6,** 351.
Delbarre, A., Muller, P., Imhoff, V. and Guern, J. (1996). Comparison of mechanisms controlling uptake and accumulation of 2,4-dichlorophenoxy acetic acid, naphthalene-1-acetic acid, and indole-3-acetic acid in suspension-cultured tobacco cells. *Planta* **198**, 532-541.
Desfeux, C., Clough, S. J. and Bent, A. F. (2000). Female reproductive tissues are the primary target of *Agrobacterium*-mediated transformation by the Arabidopsis floral-dip method. *Plant Physiol.* **123**, 895-904.
Escobar-Restrepo, J.-M., Huck, N., Kessler, S., Gagliardini, V., Gheyselinck, J., Yang, W.-C. and Grossniklaus, U. (2007). The FERONIA receptor-like kinase mediates male-female interactions during pollen tube reception. *Science* **317**, 656-660.
Evans, M. M. S. (2007). The indeterminate gametophyte1 gene of maize encodes a LOB domain protein required for embryo Sac and leaf development. *Plant Cell* **19**, 46-62.
Gallavotti, A., Yang, Y., Schmidt, R. J. and Jackson, D. (2008). The relationship between auxin transport and maize branching. *Plant Physiol.* **147**, 1913-1923.
Gallie, D. R. (2002). The 5′-leader of tobacco mosaic virus promotes translation through enhanced recruitment of eIF4F. *Nucleic Acids Res.* **30**, 3401-3411.
Garnett, P., Steinacher, A., Stepney, S., Clayton, R. and Leyser, O. (2010). Computer simulation: the imaginary friend of auxin transport biology. *BioEssays* **32**, 828-835.
Geisler, M., Blakeslee, J. J., Bouchard, R., Lee, O. R., Vincenzetti, V., Bandyopadhyay, A., Titapiwatanakun, B., Peer, W. A., Bailly, A., Richards, E. L. et al. (2005). Cellular efflux of auxin catalyzed by the Arabidopsis MDR/PGP transporter AtPGP1. *Plant J.* **44**, 179-194.
Gregor, T., Bialek, W., de Ruyter van Steveninck, R. R., Tank, D. W. and Wieschaus, E. F. (2005). Diffusion and scaling during early embryonic pattern formation. *Proc. Natl. Acad. Sci. USA* **102**, 18403-18407.
Grieneisen, V. A., Xu, J., Maree, A. F. M., Hogeweg, P. and Scheres, B. (2007). Auxin transport is sufficient to generate a maximum and gradient guiding root growth. *Nature* **449**, 1008-1013.
Gross-Hardt, R., Kägi, C., Baumann, N., Moore, J. M., Baskar, R., Gagliano, W. B., Jürgens, G. and Grossniklaus, U. (2007). LACHESIS restricts gametic cell fate in the female gametophyte of Arabidopsis. *PLoS Biol.* **5**, e47.
Guilfoyle, T. J. and Hagen, G. (2007). Auxin response factors. *Curr. Opin. Plant Biol.* **10**, 453-460.
Gutknecht, J. and Walter, A. (1980). Transport of auxin (indoleacetic acid) through lipid bilayer membranes. *J. Membr. Biol.* **56**, 65-72.
He, F., Saunders, T. E., Wen, Y., Cheung, D., Jiao, R., Rein ten Wolde, P., Howard, M. and Ma, J. (2010). Shaping a morphogen gradient for positional precision. *Biophys. J.* **99**, 697-707.
Huang, B. Q. and Sheridan, W. F. (1994). Female gametophyte development in maize: microtubular organization and embryo sac polarity. *Plant Cell* **6**, 845-861.
Johnston, A. J., Kirioukhova, O., Barrell, P. J., Rutten, T., Moore, J. M., Baskar, R., Grossniklaus, U. and Gruissem, W. (2010). Dosage-sensitive function of retinoblastoma related and convergent epigenetic control are required during the Arabidopsis life cycle. *PLoS Genet.* **6**, e1000988.
Krohn, N. G., Lausser, A., Juranić, M. and Dresselhaus, T. (2012). Egg cell signaling by the secreted peptide ZmEAL1 controls antipodal cell fate. *Dev. Cell* **23**, 219-225.
Lander, A. D., Lo, W.-C., Nie, Q. and Wan, F. Y. (2009). The measure of success: constraints, objectives, and tradeoffs in morphogen-mediated patterning. *Cold Spring Harb. Perspect. Biol.* **1**, a002022.
Liu, J., Mehdi, S., Topping, J., Tarkowski, P. and Lindsey, K. (2010). Modelling and experimental analysis of hormonal crosstalk in *Arabidopsis*. *Mol. Syst. Biol.* **6**, 373.
Ljung, K., Ostin, A., Lioussanne, L. and Sandberg, G. (2001). Developmental regulation of indole-3-acetic acid turnover in Scots pine seedlings. *Plant Physiol.* **125**, 464-475.
Marchant, A., Kargul, J., May, S. T., Muller, P., Delbarre, A., Perrot-Rechenmann, C. and Bennett, M. J. (1999). AUX1 regulates root gravitropism in Arabidopsis by facilitating auxin uptake within root apical tissues. *EMBO J.* **18**, 2066-2073.
Moll, C., von Lyncker, L., Zimmermann, S., Kägi, C., Baumann, N., Twell, D., Grossniklaus, U. and Gross-Hardt, R. (2008). CLO/GFA1 and ATO are novel regulators of gametic cell fate in plants. *Plant J.* **56**, 913-921.
Mori, Y., Jilkine, A. and Edelstein-Keshet, L. (2008). Wave-pinning and cell polarity from a bistable reaction-diffusion system. *Biophys. J.* **94**, 3684-3697.
Ottenschläger, I., Wolff, P., Wolverton, C., Bhalerao, R. P., Sandberg, G., Ishikawa, H., Evans, M. and Palme, K. (2003). Gravity-regulated differential auxin transport from columella to lateral root cap cells. *Proc. Natl. Acad. Sci. USA* **100**, 2987-2991.
Pagnussat, G. C., Yu, H.-J. and Sundaresan, V. (2007). Cell-fate switch of synergid to egg cell in Arabidopsis eostre mutant embryo sacs arises from misexpression of the BEL1-like homeodomain gene BLH1. *Plant Cell* **19**, 3578-3592.
Pagnussat, G. C., Alandete-Saez, M., Bowman, J. L. and Sundaresan, V. (2009). Auxin-dependent patterning and gamete specification in the Arabidopsis female gametophyte. *Science* **324**, 1684-1689.
Petrásek, J. and Friml, J. (2009). Auxin transport routes in plant development. *Development* **136**, 2675-2688.
Ramos, J. A., Zenser, N., Leyser, O. and Callis, J. (2001). Rapid degradation of auxin/indoleacetic acid proteins requires conserved amino acids of domain II and is proteasome dependent. *Plant Cell* **13**, 2349-2360.
Rapparini, F., Tam, Y. Y. Y., Cohen, J. D. and Slovin, J. P. (2002). Indole-3-acetic acid metabolism in *Lemna gibba* undergoes dynamic changes in response to growth temperature. *Plant Physiol.* **128**, 1410-1416.
Rotman, N., Durbarry, A., Wardle, A., Yang, W. C., Chaboud, A., Faure, J. E., Berger, F. and Twell, D. (2005). A novel class of MYB factors controls sperm-cell formation in plants. *Curr. Biol.* **15**, 244-248.
Sbalzarini, I. F., Mezzacasa, A., Helenius, A. and Koumoutsakos, P. (2005). Effects of organelle shape on fluorescence recovery after photobleaching. *Biophys. J.* **89**, 1482-1492.
Schmid, M. W., Schmidt, A., Klostermeier, U. C., Barann, M., Rosenstiel, P. and Grossniklaus, U. (2012). A powerful method for transcriptional profiling of specific cell types in eukaryotes: laser-assisted microdissection and RNA sequencing. *PLoS ONE* **7**, e29685.
Schneitz, K., Hülskamp, M. and Pruitt, R. E. (1995). Wild-type ovule development in Arabidopsis thaliana: a light microscope study of cleared whole-mount tissue. *Plant J.* **7**, 731-749.
Sequeira, L. and Mineo, L. (1966). Partial purification and kinetics of indoleacetic acid oxidase from tobacco roots. *Plant Physiol.* **41**, 1200-1208.
Shaner, N. C., Campbell, R. E., Steinbach, P. A., Giepmans, B. N. G., Palmer, A. E. and Tsien, R. Y. (2004). Improved monomeric red, orange and yellow fluorescent proteins derived from Discosoma sp. red fluorescent protein. *Nat. Biotechnol.* **22**, 1567-1572.
Srilunchang, K. O., Krohn, N. G. and Dresselhaus, T. (2010). DiSUMO-like DSUL is required for nuclei positioning, cell specification and viability during female gametophyte maturation in maize. *Development* **137**, 333-345.
Sundaresan, V. and Alandete-Saez, M. (2010). Pattern formation in miniature: the female gametophyte of flowering plants. *Development* **137**, 179-189.
Swarup, R. and Péret, B. (2012). AUX/LAX family of auxin influx carriers – an overview. *Front. Plant Sci.* **3**, 225.
Swarup, K., Benková, E., Swarup, R., Casimiro, I., Péret, B., Yang, Y., Parry, G., Nielsen, E., De Smet, I., Vanneste, S. et al. (2008). The auxin influx carrier LAX3 promotes lateral root emergence. *Nat. Cell Biol.* **10**, 946-954.
Tucker, M. R., Okada, T., Johnson, S. D., Takaiwa, F. and Koltunow, A. M. G. (2012). Sporophytic ovule tissues modulate the initiation and progression of apomixis in Hieracium. *J. Exp. Bot.* **63**, 3229-3241.
Ulmasov, T., Murfett, J., Hagen, G. and Guilfoyle, T. J. (1997). Aux/IAA proteins repress expression of reporter genes containing natural and highly active synthetic auxin response elements. *Plant Cell* **9**, 1963-1971.
Vernoux, T., Brunoud, G., Farcot, E., Morin, V., Van den Daele, H., Legrand, J., Oliva, M., Das, P., Larrieu, A., Wells, D. et al. (2011). The auxin signalling network translates dynamic input into robust patterning at the shoot apex. *Mol. Syst. Biol.* **7**, 508.
Weijers, D., Schlereth, A., Ehrismann, J. S., Schwank, G., Kientz, M. and Jürgens, G. (2006). Auxin triggers transient local signaling for cell specification in Arabidopsis embryogenesis. *Dev. Cell* **10**, 265-270.
Xiang, C., Han, P., Lutziger, I., Wang, K. and Oliver, D. J. (1999). A mini binary vector series for plant transformation. *Plant Mol. Biol.* **40**, 711-717.
Xu, T., Wen, M., Nagawa, S., Fu, Y., Chen, J.G., Wu, M.J., Perrot-Rechenmann, C., Friml, J., Jones, A.M., and Yang, Z. (2010). Cell surface- and Rho GTPase-based auxin signaling controls cellular interdigitation in Arabidopsis. *Cell* **143**, 99-110.
Yanagisawa, S. and Sheen, J. (1998). Involvement of maize Dof zinc finger proteins in tissue-specific and light-regulated gene expression. *Plant Cell* **10**, 75-89.
Yang, Y., Hammes, U. Z., Taylor, C. G., Schachtman, D. P. and Nielsen, E. (2006). High-affinity auxin transport by the AUX1 influx carrier protein. *Curr. Biol.* **16**, 1123-1127.

APPENDIX 1

(Lituiev et al. 2013, Development 140)

SUPPLEMENTARY TEXT

Simulation conditions and parameter values

The reaction-diffusion model described in the main text was studied in the form of a partial differential equation with boundary conditions:

$$\frac{\partial u}{\partial t} = D \cdot \nabla^2 u - \hat{a} \cdot u + \hat{b}$$

$$\nabla u|_{\Gamma_1} = -\hat{p}$$

$$\nabla u|_{\Gamma_2} = -\hat{q} \cdot u$$

Where u is the auxin concentration, D is the diffusion coefficient, $\hat{a}$ is the degradation rate, $\hat{b}$ is the synthesis rate, $\hat{p}$ is the influx rate, and $\hat{q}$ is efflux rate, Γ_1 is the boundary domain of influx (micropyle, $x = 0$ in one dimension) and Γ_2 is the boundary domain of efflux (chalaza, $x = 1$ in one dimension). The ∇ sign represents the gradient operation (first spatial derivative), and ∇^2 is the Laplacian operator (second spatial derivative). The equation thus describes the local instanteneous change of the auxin concentration, which is influenced by the diffusion ($D \cdot \nabla^2 u$ term), degradation (-$\hat{a}\,u$), and synthesis ($\hat{b}$).

Further, we rescale the degradation rate and the efflux rate by the length (L) of the female gametophyte (FG) and diffusion rate (D); the rescaled degradation rate becomes $a = \hat{a} \cdot \frac{L^2}{D}$ and the rescaled efflux rate $q = \hat{q} \cdot \frac{L}{D}$. As the differential equation is linear, the influx rate and synthesis rate can be selected arbitrary. We chose these parameters such to equal the mean concentration of auxin with the value of one.

One-dimensional solutions were found analytically and were simulated using MATLAB software. We set the *pdepe* function for non-negative solutions, and used otherwise standard numeric settings (relative error tolerance 10^{-3}, absolute error tolerance 10^{-6}), unless otherwise specified. The values used are shown in Table S4.

Two-dimensional simulations using the COMSOL software package were carried out with a relative error tolerance of 10^{-7}. For both one- and two-dimensional models, we assumed homogeneous and isotropic auxin diffusion throughout the cytoplasm and apoplastic space. This is an approximation, as the presence of cellular compartments can slow down diffusion by about 4-fold (Sbalzarini et al., 2005), and the presence of cytoplasmic streaming can increase the effective transport rate. Degradation of auxin was assumed to be homogeneous throughout the cytoplasm (or part of it in regime 3). The key parameter grouping of the model under these assumptions is the rescaled characteristic length scale of degradation λ/L, whose estimated values are presented in the Table S1.

Arabodpisis and maize FG lengths were measured from pictures using ImageJ software. The distribution of FG lengths is shown in Fig. S7.

In order to assess the width of the cytoplasmic isthmus, we analyzed *Arabidopsis* wild-type (L*er*) plants expressing a membrane-localized GFP under the control of an FG-specific promoter (*pAtD123::EGFP-AtROP6C*, Escobar-Restrepo et al., 2007). As shown in Fig. S8, the width of the isthmus is in the order of 1 μm.

Estimation of the membrane permeability parametes.

We estimated auxin flux parameters from the data of Geisler et al. (2005). We assumed the following:

1. Linear dependence of the auxin trans-membrane flux on auxin concentration. This assumption can be justified by the fact that the auxin concentration applied in the experiment (500 nM) is lower than the known Km for the auxin transporters (more than 840 nM; Yang et al., 2006; Swarup et al., 2008).
2. Fast diffusion rate compared to transport. The data suggests that the assumption holds because the characteristic diffusion time (the ratio of the diffusion coefficient to the protoplast radius) is around $6 \cdot 10^{-5}$ m/s, with diffusion coefficient of $6 \cdot 10^{-10}$ m^2/s (Grieneisen et al, 2007), while the estimated transmembrane flux values are slower than 10^{-8} m/s.
3. Background auxin in- and efflux are mediated by the protonated form only.
4. The effect of vacuolar trapping is insignificant.
5. Auxin flux in wild-type protoplasts kept in the dark does not involve any auxin transporter proteins.

6. PGP1 activity in mesophyll protoplasts is the same as in the FG.
7. As no auxin efflux carriers except for PGP1 are expressed in the FG, similarly to the *pgp19* mutant, we used the estimate of the transport rate in *pgp19* mutant protoplasts for further simulations of the wild-type FG.

Based on these assumptions we made the following estimations: the auxin efflux rate in the *pgp19* mutant is $1.1 \cdot 10^{-8}$ m/s; net passive auxin efflux (wild-type protoplasts in darkness) $5.6 \cdot 10^{-9}$ m/s; net passive auxin influx $4.3 \cdot 10^{-8}$ m/s; and the permeability of the membrane to the protonated form of auxin $1.3 \cdot 10^{-6}$ m/s.

Note that the parameter values for passive auxin flux, estimated based on the data by Geisler et al. (2005), indicate a lower membrane permeability in *Arabidopsis* protoplasts compared to the one estimated earlier by Gutknecht and Walter (1980) for lecitine bilayer membranes. However, we used the former, as they are obtained in a biological, and thus more relevant system for our studies.

Geometrical features of the two-dimensional model

For this model, we assumed that key properties of the FG can be described by the following geometry:

1. The shape of the FG is approximated by an ellipsoid.
2. The large central vacuole is represented by an intersection of an ellipsoid whose both semiradii are less than the semiradii of the FG by the value of Δy and a shpere of radius 1/3.
3. The apoplast is modeled as a space between the plasma membrane of the FG and another membrane located at distance of Δw from it, representing the plasma membranes of surrounding sporophytic cells.
4. The influx of auxin occurs in the micropylar pole of the plasma membrane of a surrounding cell.
5. The concentration of protonated auxin at the plasma membrane of cells located at the chalazal half of the FG is set to zero.

The geometry is thus axi-symmetrical two-dimensional. The values of the geometric parameters are presented in the Table S5.

Antagonistic auxin fluxes occur during polarization of germ lineage cells

The auxin efflux carrier ZmPIN1a of maize was expressed as YFP fusion protein under control of the endogenous promoter (Gallavotti et al., 2008) to study the auxin flux occurring during ovule and germline development. As shown in Fig. 7M of the main text and in Fig. S2A,B, auxin flux as indicated by the polar localization of ZmPIN1a is directed at the tip of the ovule primordium towards the micropylar pole of the primordial germ cell (PGC) and megaspore cell (MSC), but is removed from the chalazal pole towards the ovule axis. After meiosis, ZmPIN1a localization at the micropylar pole starts to disappear, becoming very weak already at stage FG2/3 (Fig. S2C,D). In contrast, expression increased at the chalazal pole, presumably directing auxin towards the axis of the developing ovule and removing it from the chalazal pole of the developing FG. Strong ZmPIN1a-YFP signals were observed in nucellus cells surrounding the chalazal pole of the FG at stage FG5 (Fig. 7N of main text and Fig. S2E,F), when cellularization and separation of gametic and accessory cells occurs. During proliferation of antipodal cells, ZmPIN1a-YFP signals were also detectable inside these cells (Fig. 7O of main text and Fig. S2G,H) and appeared to accumulate in endosomes of antipodal cells within fully mature FGs (Fig. S2I,J). Whether auxin was removed from the chalazal pole of the maturing central cell could not be definitely determined, but as shown by *DR5* promoter activity, the highest auxin response was observed in the antipodal cell most distant from the central cell (Fig. 7K of main text and Fig. S13D), indicating that auxin flux is likely kept low in the immediate surrounding of the central cell.

Sensitivity analysis

Independent parameter groups taken into analysis. The mathematical model under regime 4 contains 12 linearly independent non-dimensional groupings.

1. Cytoplasmic isthmus width Δy_{cyt} (Table S5)
2. Apoplast isthmus width Δy_{apo} (Table S5)
3. Vacuole length r_{vac} (Table S5)

4. Width *B* of the FG (Table S5)

5. Characteristic degradation rate (regarded as a ratio between the degradation velocity $\hat{q}_a := \hat{a} \cdot L$ and the diffusion velocity $\hat{q}_D := \frac{D}{L}$, and equivalent to the inverse of squared rescaled characteristic degradation length scale)

$$a = \frac{\hat{q}_a}{\hat{q}_D} = \hat{a} \cdot \frac{L^2}{D} = \left(\frac{\lambda}{L}\right)^{-2}$$

6. Rescaled active efflux rate of auxin from the cytoplasm to apoplast:

$$q_{c-a} = \frac{\hat{q}_{c-a}}{\hat{q}_D}$$

7. Characteristic dissociation velocity of auxin: $\beta := \frac{\hat{\beta}}{\hat{a}}$

8. Rescaled passive flux rate for protonized auxin: $q_{IAAH} = \frac{\hat{q}_{IAAH}}{\hat{q}_D}$

9. pKd of auxin

10. pH of the vacuole

11. pH of the cytoplasm

12. pH of the apoplast

The rate parameters here are normalized with respect to the characteristic diffusion velocity ($\hat{q}_D = \frac{D}{L}$), while the geometrical parameters are normalized with respect to the FG length *L*. *D* represents diffusion rate, the FG length *L*, and $\hat{a}$ is degradation rate in natural dimensions.

Alternatively, given fast auxin dissociation, six parameters influencing auxin flux (7—12) can be collected into three following parameters:

7.a. Rescaled influx from the apoplast to the cytoplasm $q_{a—c}$;

8.a. Rescaled efflux from the vacuole to the cytoplasm $q_{v—c}$;

9.a. Rescaled influx from the cytoplasm to the vacuole $q_{c—v.}$

Calculation of the sensitivity. The robustness and sensitivity of the morphogen gradient can be addressed by studying how the perceived threshold concentration (x_{thr}) is shifted upon the perturbation in the parameter values (α). Namely, we are interested in the fixed (threshold) level of the morphogen concentration at the physiological parameter value (α_0) (de Lachapelle and Bergmann 2010). The sensitivity of the solution to deviation in the parameter values (α) can be estimated from the full derivative formula:

$$\frac{\mathrm{d}u}{\mathrm{d}x} = \frac{\partial u}{\partial x}\cdot\frac{\mathrm{d}x}{\mathrm{d}x} + \frac{\partial u}{\partial \alpha}\cdot\frac{\mathrm{d}\alpha}{\mathrm{d}x} + o\left(\frac{1}{2}\cdot\frac{\partial^2 u}{\partial x^2} + \frac{1}{2}\cdot\frac{\partial^2 u}{\partial \alpha^2}\cdot\left(\frac{\mathrm{d}\alpha}{\mathrm{d}x}\right)^2\right) \qquad (*)$$

We are interested in the effects of finitesimally small shifts in the values of du, dx, and dα which according to (*) are approximately related as follows:

$$\mathrm{d}u \approx \frac{\partial u}{\partial x}\cdot \mathrm{d}x + \frac{\partial u}{\partial \alpha}\cdot \mathrm{d}\alpha$$

At this stage we can address the *sensitivity of the concentration to the changes in the parameter values*, i.e. how the concentration in some point x_0 (dx = 0) will be shifted upon perturbation dα (Fig. S9). Dividing both sides by u_0 we obtain:

$$\frac{\mathrm{d}u}{u_0} \approx \left.\frac{\partial \ln u}{\partial \ln \alpha}\right|_{\alpha_0, u_0}\cdot\frac{\mathrm{d}\alpha}{\alpha_0} \equiv \varepsilon_{u\alpha}\cdot\frac{\mathrm{d}\alpha}{\alpha_0}$$

Where $\varepsilon_{u\alpha}$ is the coefficient of sensitivity of concentration to the parameter values.

Then, we can question the *sensitivity of the threshold position to the concentration*, i.e. how the position of the threshold concentration will move if the concetration is changed under the fixed parameter values:

$$dx \approx \left(\frac{\partial \ln u}{\partial x}\Big|_{u_0,x_0}\right)^{-1} \cdot \frac{du}{u_0} \equiv \varepsilon_{ux} \cdot \frac{du}{u_0}$$

Where ε_{ux} is the coefficient of sensitivtiy of the threshold position to the concentration. One can notice that it is given by the concentration value divided by the gradient at a given point:

$$\varepsilon_{ux} = u_0 \,/\, \frac{\partial u}{\partial x}\Big|_{x_0}$$

Further, we can study the *sensitivity of the threshold position to the perturbation in the parameter value*, i.e. how some position at which concentration is equal to some threshold concentration u_0 ($du = 0$) will shift upon perturbation in the parameter vale $d\alpha$:

$$dx \approx \left(\frac{\partial \ln u}{\partial x}\Big|_{u_0,x_0}\right)^{-1} \cdot \frac{\partial \ln u}{\partial \ln \alpha}\Big|_{\alpha_0,u_0} \cdot \frac{d\alpha}{\alpha_0} \equiv \varepsilon \cdot \frac{d\alpha}{\alpha_0}$$

Where $\varepsilon = \varepsilon_{ux} \cdot \varepsilon_{u\alpha}$. Particularly, as the partial differential equation under consideration is linear, the sensitivity of the concentration to the source intensity (the concentration of auxin at the micropylar pole) is equal to one ($\varepsilon_{u\alpha} = 1$), i.e. the sensitivity of the threshold position to the perturbation in the source is equivalent to the sensitivity to the perturbation in concentration.

The sensitivity of the concentration to changes in the parameter values. The concentration is highly sensitive to the changes in the pH of the apoplast and the source (i.e. auxin concentration in the neighbouring cells at the micropylar pole). Perturbations in these former parameters will be amplified by about 10 times. The perturbation in the rest of the parameters will be dampened, however (Table S2).

The sensitivity of the threshold position to the concentration change. The threshold position could not be correctly distinguished in the micropylar part (i.e. it is shifted out of the FG) if the perturbation in the auxin concentration exceeds around 1%. With perturbations higher than 3.5%, the threshold determination becomes impossible also in the chalazal part (see Fig. 5 in the main text).

The sensitivity of the threshold position to the perturbation in the parameter value can be found as the product of the two previously mentioned sensitivity coefficient.

REFERENCES

Abbruzzetti, S., Grandi, E., Viappiani, C., Bologna, S., Campanini, B., Raboni, S., Bettati, S. and Mozzarelli, A. (2005). Kinetics of acid-induced spectral changes in the GFPmut2 chromophore. *J. Am. Chem. Soc.* **127**, 626–635.

Chavarría-Krauser, A. and Ptashnyk, M. (2010). Homogenization of long-range auxin transport in plant tissues. *Nonlinear Anal. Real World Appl.* **11**, 4524–4532.

Escobar-Restrepo, J.-M., Huck, N., Kessler, S., Gagliardini, V., Gheyselinck, J., Yang, W.-C. and Grossniklaus, U. (2007). The FERONIA receptor-like kinase mediates male-female interactions during pollen tube reception. *Science*. **317**, 656–660.

Gallavotti, A., Yang, Y., Schmidt, R. J. and Jackson, D. (2008). The relationship between auxin transport and maize branching. *Plant Physiol.* **147**, 1913–1923.

Grieneisen, V. A., Xu, J., Maree, A. F. M., Hogeweg, P. and Scheres, B. (2007). Auxin transport is sufficient to generate a maximum and gradient guiding root growth. *Nature* **449**, 1008–1013.

Gutknecht, J. and Walter, A. (1980). Transport of auxin (indoleacetic acid) through lipid bilayer membranes. *J. Membr. Biol.* **56**, 65–72.

Liu, J., Mehdi, S., Topping, J., Tarkowski, P. and Lindsey, K. (2010). Modelling and experimental analysis of hormonal crosstalk in *Arabidopsis*. *Mol. Syst. Biol.* **6**.

Ljung, K., Ostin, A., Lioussanne, L. and Sandberg, G. (2001). Developmental regulation of indole-3-acetic acid turnover in Scots pine seedlings. *Plant Physiol.* **125**, 464–475.

Mravec, J., Kubes, M., Bielach, A., Gaykova, V., Petrásek, J., Skůpa, P., Chand, S., Benková, E., Zazímalová, E. and Friml, J. (2008). Interaction of PIN and PGP transport mechanisms in auxin distribution-dependent development. *Development* **135**, 3345–3354.

Rapparini, F., Tam, Y. Y. Y., Cohen, J. D. and Slovin, J. P. (2002). Indole-3-acetic acid metabolism in *Lemna gibba* undergoes dynamic changes in response to growth temperature. *Plant Physiology* **128**, 1410–1416.

Sequeira, L. and Mineo, L. (1966). Partial purification and kinetics of indoleacetic acid oxidase from tobacco roots. *Plant physiology* **41**, 1200–1208.

Slifkin, M. (1984). Protonation rate constants of proline. *J. Mol. Liq.* **29**, 75–80.**Slifkin, M. A. and Ali, S. M.** (1991). Thermodynamic and rate parameters for alanine protonation reactions. *J. Chem. Soc., Faraday Trans.* **87**, 3241–3243.

SUPPLEMENTARY TABLES

Table S1. Values of degradation rate and corresponding gradient steepness at regime 1

Ref.	Object	Degradation rate, $\hat{a}$	Half-life	a	λ/L	GS
(Sequeira and Mineo,1966)	Tobacco leaf protoplasts	$5\cdot10^{-4}$	23 min	$4.08\cdot10^{-3}$	15.6	0.204%
(Ljung et al., 2001)	Scots pine seedlings	$2.67\cdot10^{-5}$	7.2 h	$2.18\cdot10^{-4}$	67.7	0.0109%
(Rapparini et al., 2002)	*Lemna gibba* (aquatic monocot)	$<1.93\cdot10^{-3}$	<6 min	$1.58\cdot10^{-2}$	7.97	0.783%
(Grieneisen et al.,2007)	Model fitting	$5\cdot10^{-6}$	3.85 h	$4.08\cdot10^{-5}$	156	0.00204%
(Liu et al., 2010)	Model fitting	2	0.35 s	$1.63\cdot10^{1}$	0.247	96.49%

Table S2. Sensitivity of the model to perturbation in parameters (regime 4 in two dimensions). For description of parameters see Table 2 and 3.

Parameter	median of $\|\varepsilon\|$	maximum of $\|\varepsilon\|$
Δy	$2.66 \cdot 10^{-2}$	$3.98 \cdot 10^{-2}$
w	$1.15 \cdot 10^{-2}$	$1.91 \cdot 10^{-2}$
B	$4.85 \cdot 10^{-5}$	$6.56 \cdot 10^{-5}$
r_{vac}	$8.79 \cdot 10^{-4}$	$4.91 \cdot 10^{-3}$
s	$1.67 \cdot 10^{-2}$	$2.94 \cdot 10^{-2}$
D	$6.57 \cdot 10^{-3}$	$9.78 \cdot 10^{-3}$
$k_{\mathrm{AUX1}}^{\mathrm{micr}}$	$2.00 \cdot 10^{-2}$	$2.98 \cdot 10^{-2}$
$q_{c\text{-a}}$	$6.08 \cdot 10^{-5}$	$7.24 \cdot 10^{-5}$
$q_{\mathrm{a\text{-}c}}$	$1.50 \cdot 10^{-2}$	$2.26 \cdot 10^{-2}$
$q_{\mathrm{c\text{-}v}}$	$2.62 \cdot 10^{-4}$	$2.85 \cdot 10^{-4}$
$q_{\mathrm{v\text{-}c}}$	$7.50 \cdot 10^{-4}$	$1.94 \cdot 10^{-3}$
p_{IAA}	$1.50 \cdot 10^{-2}$	$2.26 \cdot 10^{-2}$
K	$1.40 \cdot 10^{-3}$	$2.34 \cdot 10^{-3}$
$\mathrm{pH}_{\mathrm{apo}}$	$1.36 \cdot 10^{-3}$	$2.31 \cdot 10^{-3}$
$\mathrm{pH}_{\mathrm{cyt}}$	$2.41 \cdot 10^{-3}$	$2.65 \cdot 10^{-3}$
$\mathrm{pH}_{\mathrm{vac}}$	$1.21 \cdot 10^{-2}$	$3.11 \cdot 10^{-2}$

Table S3. The *p*-value of the one-sided Wilcoxon signed rank test with the alternative hypothesis that the $\log_2$ fluorescence ratios in the ovules of the degron plants (pUBQ10:degron-GFP) are higher than in ovules of the control plants (pUBQ10:degron-GFP).

Stage	$\log_2$[ES / integument]	$\log_2$[ES / nucellus]	$\log_2$[integument / nucellus]
FM	0.1397	0.0005 *	0.0026 *
FG3	0.7665	0.1409	0.0033 *

* significant within 0.05 confidence interval

Table S4. Reaction, diffusion and transport parameters

Abbreviation	Parameter	Value	Reference
a	dimensionless degradation rate	0.0158	
λ/L	rescaled characteristic length scale	$a^{-1/2} = 7.97$	
β	dimensionless protonation rate	$8.33 \cdot 10^4$	
pH_{apo}	apoplastic pH	5.00	
pH_{cyt}	cytoplasmatic pH	7.60	(Chavarría-Krauser and Ptashnyk, 2010)
pK_d	IAA dissociation constant	4.75	(Chavarría-Krauser and Ptashnyk, 2010)
k_d	dissociation rate (estimation for auxin)	1.4·106 s-1	(Chavarría-Krauser and Ptashnyk, 2010)
$P_{[HA]}$	permeability to non-ionized auxin	$4.8 \cdot 10^{-6}$ m/s	(Geisler et al., 2005)
$P_{[A-]}$	permeability to ionized auxin	$<10^{-11}$ m/s	(Gutknecht and Walter, 1980)
q_1	dimensionless membrane permeability to IAAH	5.50	
q_2	dimensionless membrane permeability to IAA^-	$1.67 \cdot 10^{-6}$	
v_1	dimensionless IAAH diffusion coefficient in the membrane	$q_1 \times \Delta x = P_1 \Delta \hat{x}/D$	
v_2	dimensionless IAA^- diffusion coefficient in the membrane	$q_2 \times \Delta x$	

b^{ES}_{IAA}	auxin production rate in the ES (NCAS model)	{0,2,3}	
$b^{adj.c.}_{IAA}$	auxin production rate in the adjacent cells (NCAS model)	0.189	
c_{thr}	threshold of [IAA] for NCAS promoter activation	0.189	
$b^{adj.c.}_{NCAS}$	NCAS production rate in the adjacent cells	5	
a_{NCAS}	NCAS degratation rate in the cytoplasm	30	
D_{NCAS}	NCAS diffusion coefficient	0.05	

Table S5: Geometric parameter values

Abbrev.	Value	Description
L	70 μm	*A. thaliana* FG length at FG5 stage
$\Delta\hat{x}$	5 nm	membrane width
Δx	$\Delta\hat{x}/L$	dimensionless membrane width
$\Delta\hat{y}$	1 μm	width of cytoplasmic path around the vacuole
Δy	$\Delta\hat{y}/L$	dimensionless width of cytoplasmic path around the vacuole
$\hat{w}$	50 nm	the width of the apoplast
w	$\hat{w}/L$	rescaled width of the apoplast
s	$L/10$	the localization of the sporophytic cells providing the source of auxin
B	2/5 L	FG width-to-length ratio
r_{vac}	2/3 L	vacuole length

FIGURES

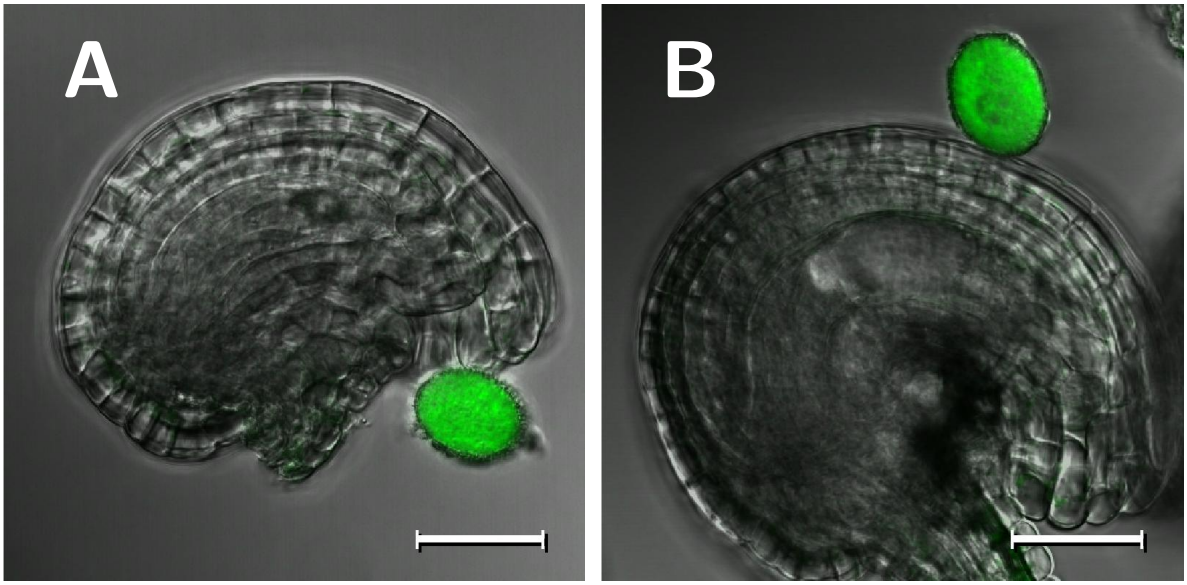

Fig. S1. PIN8 protein is not detected in the *Arabidopsis* ovules. Ovules and pollen from plants carrying PIN8::PIN8:GFP promoter-fusion construct were analysed. While a PIN8:GFP signal is clearly observed in the pollen grains as expected, no signal can be detected in ovules during FG4 (**A**) and FG6 (**B**) stages. Scale bars: 30 μm.

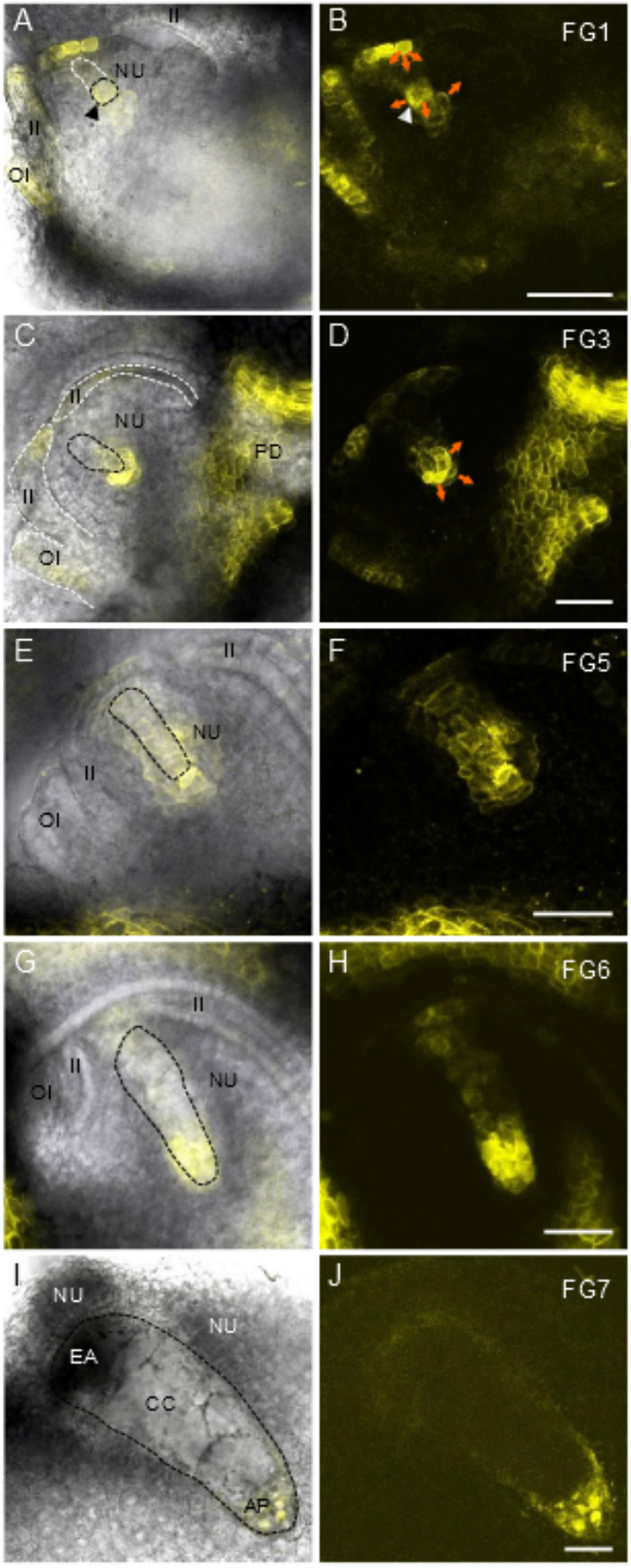
A
II
NU
II
OI
B
FG1
C
II
NU
PD
II
OI
D
FG3
E
II
NU
II
OI
F
FG5
G
II
II
OI
NU
H
FG6
I
NU
NU
EA
CC
AP
J
FG7

Fig. S2 *(preceding page)*. Localization of the auxin efflux carrier ZmPIN1a during ovule development in maize. ZmPIN1a was expressed as a YFP fusion protein under control of its endogenous promoter. Orange arrows indicate the predicted auxin flux according to polarized ZmPIN1a localization. (**A**) A female gametophyte at stage FG1 (shortly after meiosis): ZmPIN1a-YFP is localized at the plasma membrane of micropylar nucellus cells pointing towards the degenerating megaspores (encircled by a white dashed line) as well as around the functional megaspore (indicated by a black dashed line and arrowhead). Additionally, ZmPIN1a-YFP is visible in the developing integuments. (**B**) Fluorescence image of (A). The arrowhead points towards the position of the functional megaspore. (**C**) Stage FG3: ZmPIN1a-YFP is no longer detectable at micropylar nucellus cells. YFP signals in nucellus cells, surrounding the chalazal pole of the female gametophyte, have increased in intensity. Additionally, ZmPIN1a-YFP is visible in the integuments and strongly in the pedicel cells differentiating vascular tissue. Note that the pericarp was removed. (**D**) Fluorescence image of (C). (**E**) Stage FG5: ZmPIN1a-YFP signals are strongest in nucellus cells surrounding the chalazal pole of the female gametophyte. (**F**) Fluorescence image of (E). (**G**) Stage FG6: ZmPIN1a-YFP signals are strongest in nucellus cells surrounding and inside antipodal cells. (H) Fluorescence image of (G). (**I**) Mature stage FG7: Integuments were removed. ZmPIN1a-YFP signals inside antipodal cells seem to be mainly localized to the endosomal compartment. (**J**) Fluorescence image of (I). (A, C, E, G and I) merged bright field and fluorescence images. The female gametophyte is indicated by a black dashed line. Abbreviations: AP: antipodal cells, CC: central cell, EA: egg apparatus, II: inner integument, NU: nucellus, OI: outer integument, PD: pedicel. Scale bars: 50 μm.

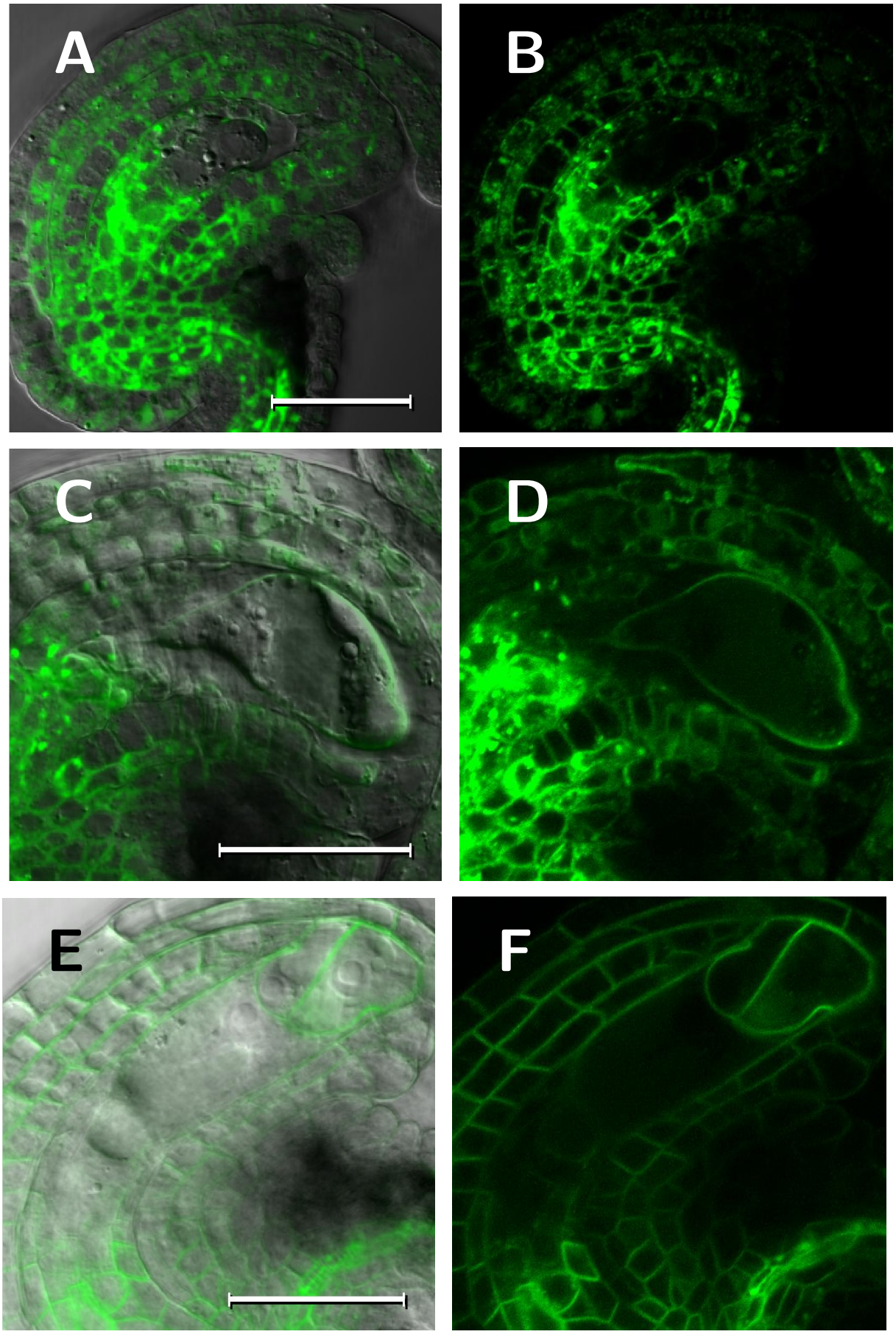
A
B
C
D
E
F

Fig. S3 *(preceding page)*. PGP1 is expressed and evenly distributed over the plasma membrane in the *Arabidopsis* female gametophyte. (**A, B**) FG3 stage: PGP1:GFP is highly expressed in the sporophytic tissue in the chalazal part of the nucellus, a moderate signal is also observed within the two-nucleate FG, (**C, D**) FG4 stage: the strong PGP1:GFP signal remains in the chalazal part of the nucellus; the almost uniform staining in the plasma membrane of the four-nucleate FG becomes more distinct; (**E, F**) FG6 stage: strong PGP1:GFP expression can now be observed within the synergid (the cell on the right in the top right corner) and the egg cell (the cell on the left). (A, C, and E) Overlay of the DIC and GFP channels; (B, D, and F) corresponding GFP channel alone. The samples A, B, and C, D were plasmolysed and cleared with the 1M glycin solution to better visualize the localization in the FG membrane. Scale bars: 30 μm.

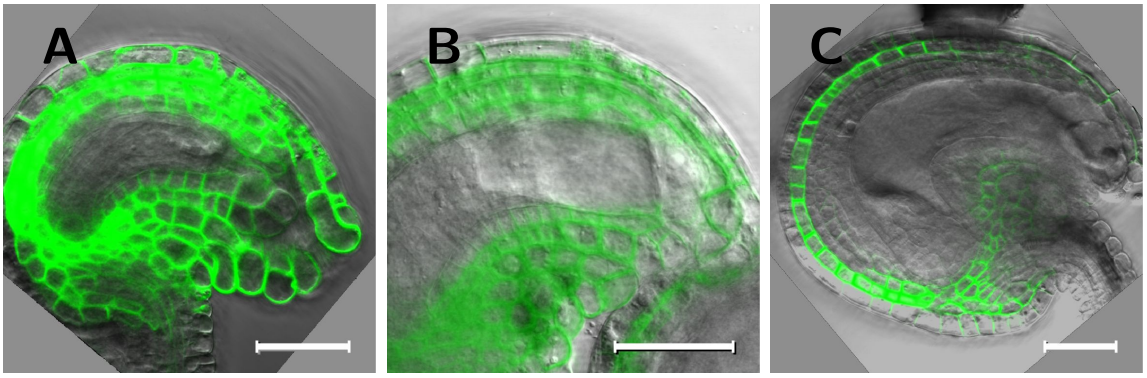

Fig. S4. PGP19 is expressed in the sporophytic tissues of the *Arabidopsis* ovules. (**A**) functional megaspore stage (FG1) and (**B**) FG6 stage: PGP19:GFP is expressed in the inner and outer integuments. (C) FG7 stage: PGP19:GFP is localized to the subepidermal cell layer only. Scale bars: 30 μm.

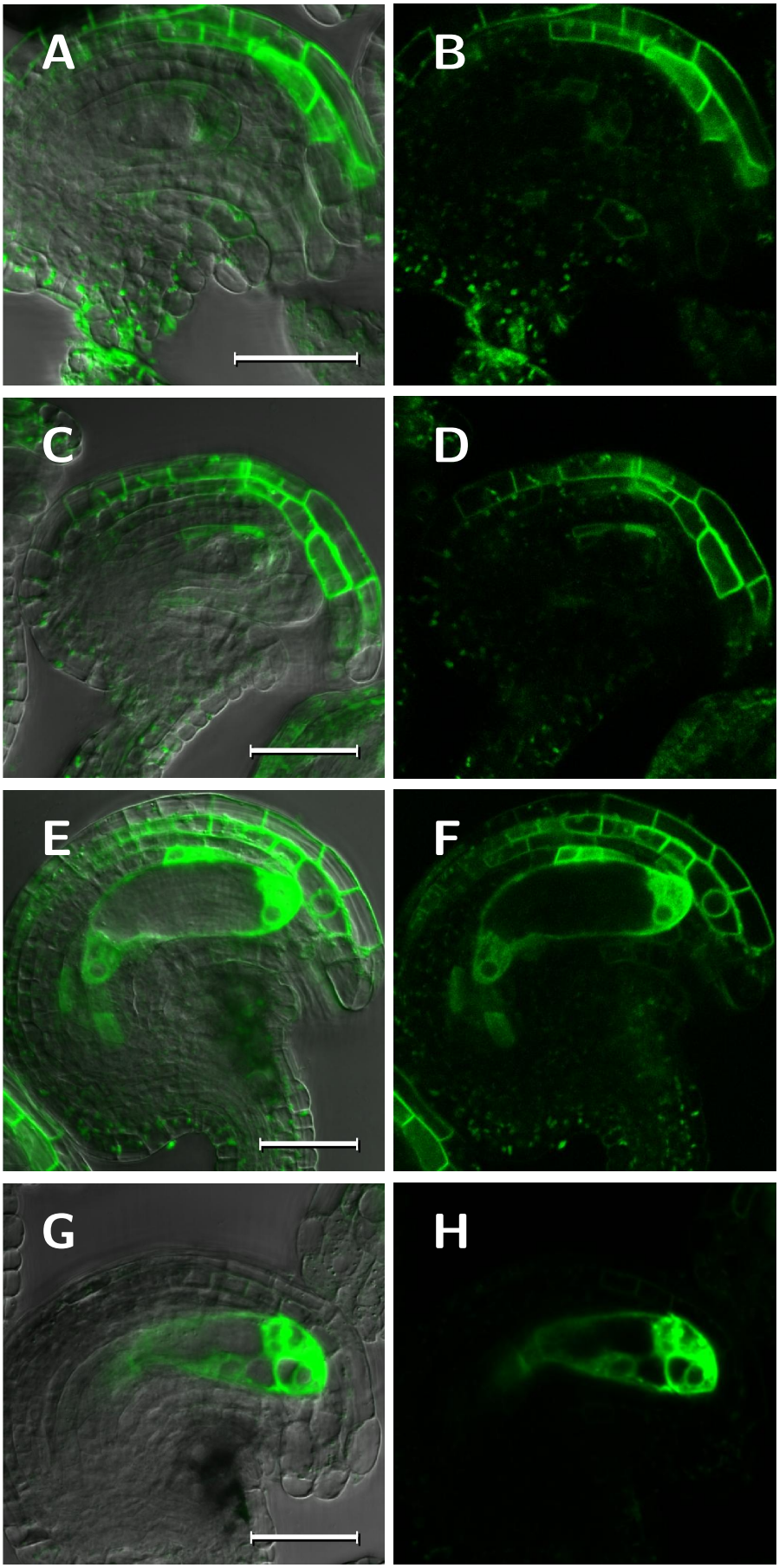
A
B
C
D
E
F
G
H

Fig. S5 *(preceding page).* AUX1 is expressed and polarly distributed in the plasma membrane in the *Arabidopsis* female gametophyte from the FG4 stage onward. (**A, B**) FG2 stage: AUX1:YFP is strongly expressed within the upper part of the outer integument and, at a lower extent, the sporophytic tissue of the nucellus. (**C, D**) FG3 stage: AUX1:YFP expression becomes stronger in the nucellus. (**E, F**) FG4 stage: AUX1:YFP expression appears within the FG first at the four-nulceate stage, with the YFP intensity in the micropylar compartment approximately 5 times higher than in the chalazal one; expression within the endothelium becomes stronger; some expression appears also in the chalazal part of the nucellus. (**G, H**) FG7 stage: AUX1:YFP expression becomes stongest in the cells of the FG, with signal in the surrounding tissues becoming undetectable. (A, C, E and G) Overlay of the DIC and GFP channels; (B, D, F and H) corresponding GFP channel alone. Scale bars: 30 μm.

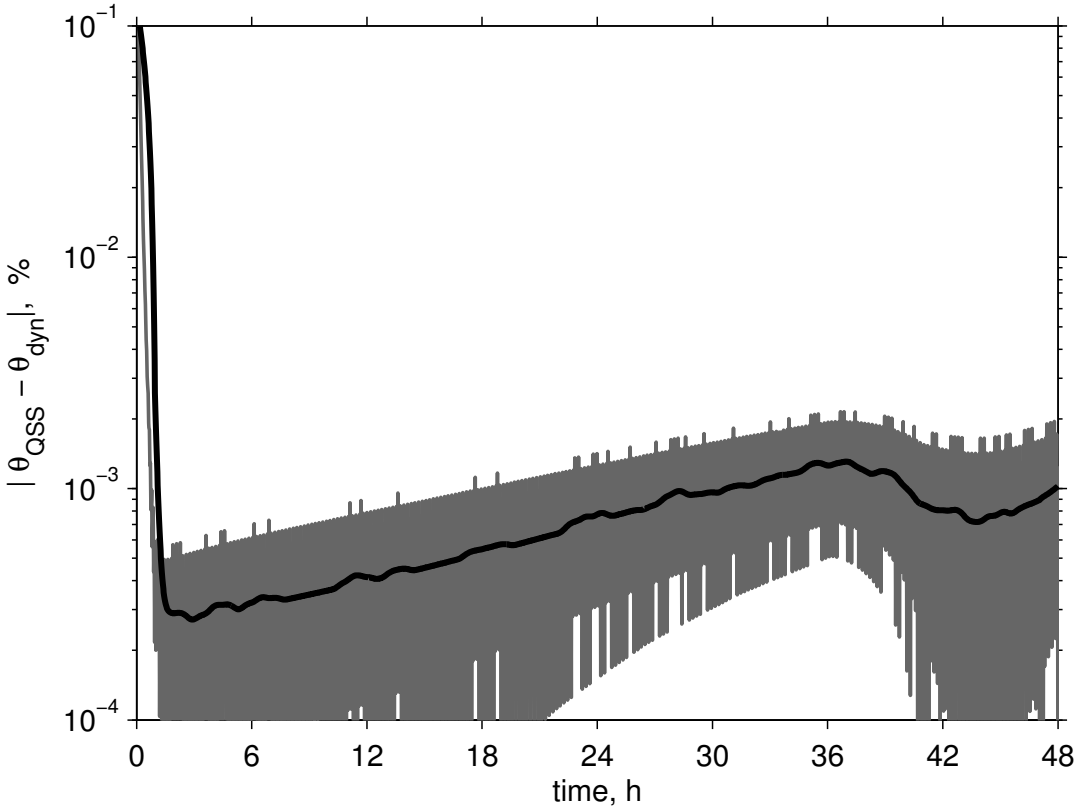

Fig. S6. Numerical studies suggest that a quasi-steady state assumption about growth leads to a negligibly small error in regime 1. The absolute value of difference between the gradient steepness found as quasi-steady state and dynamic solution $|\theta_{\mathrm{QSS}} - \theta_{\mathrm{dyn}}|$ expressed in percentage points. Note that the absolute value of the difference does not exceed 0.0022% after initial equilibration during the first 38 minutes. The original data (gray line) was smoothened with a moving average filter with window size of two hours (black line). The relative error tolerance of the ODE solver was set to 10^{-5}.

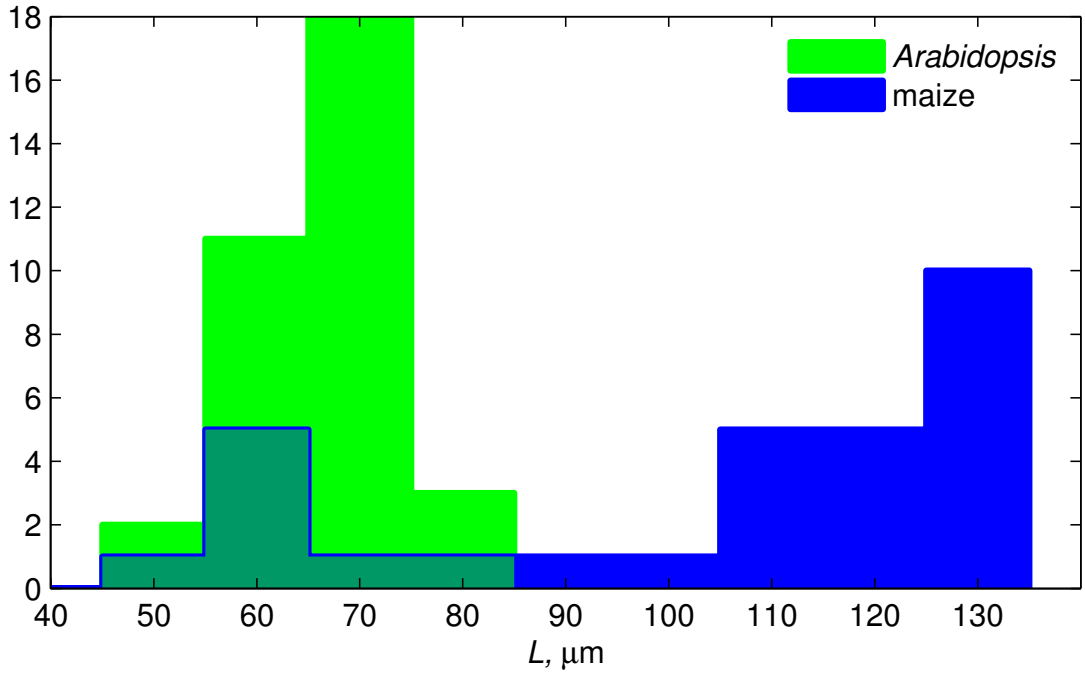

Fig. S7. Distribution of the female gametophyte lengths in Arabidopsis and maize at stage FG4/5. The graph shows the distribution of FG lengths (in µm) measured from micrographs. *Arabidopsis* is shown in green, maize in blue

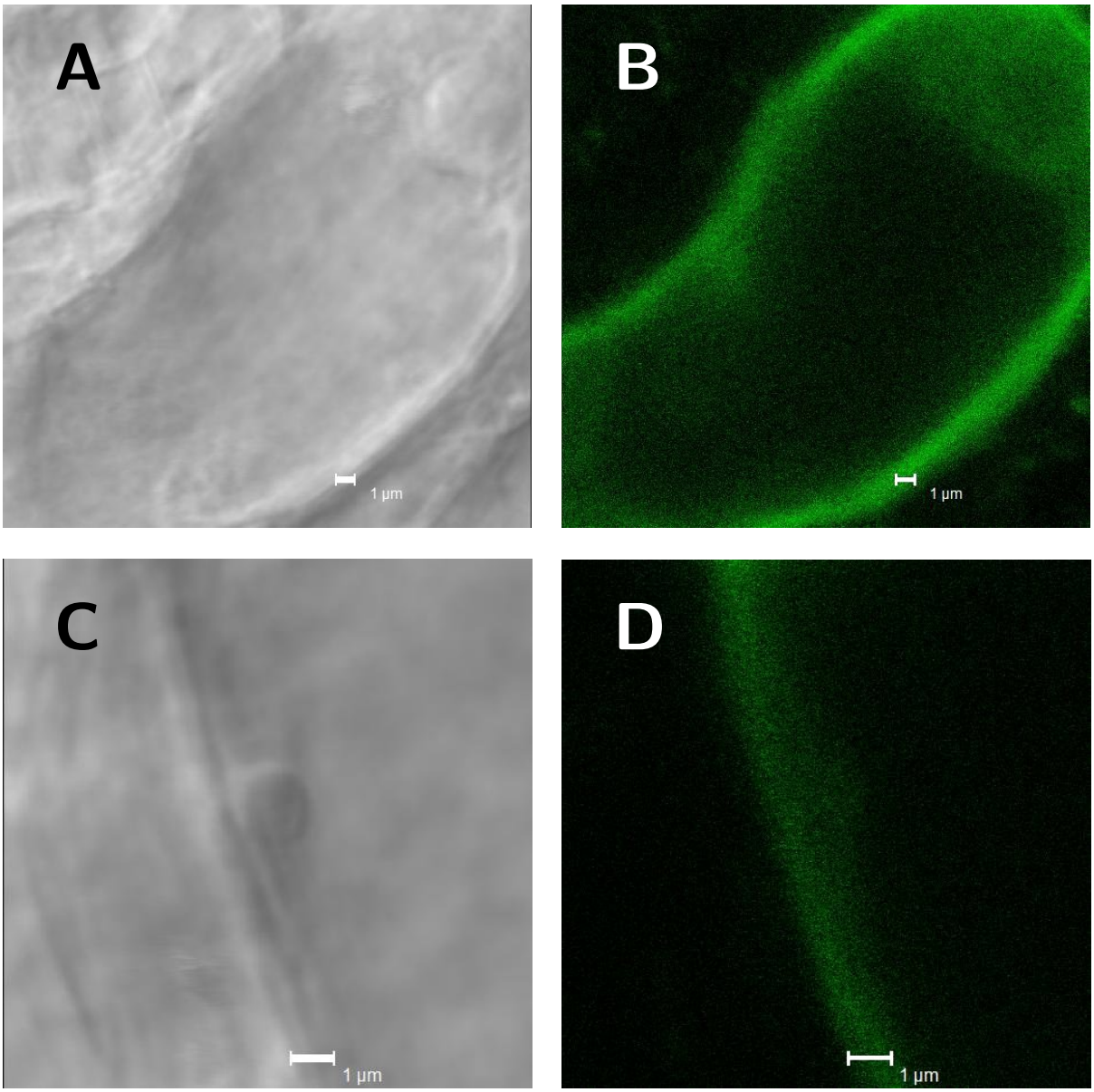

Fig. S8. The isthmus between central vacoule and female gametophyte membranes. (**A, C**) Differential interference contrast of *Arabidopsis* wild-type FG4 FGs. (**B, D**). Fluorescent micrographs of the same ovules expressing a membrane-localized GFP driven by an FG-specific promoter. The isthmus is around 1 µm in width.

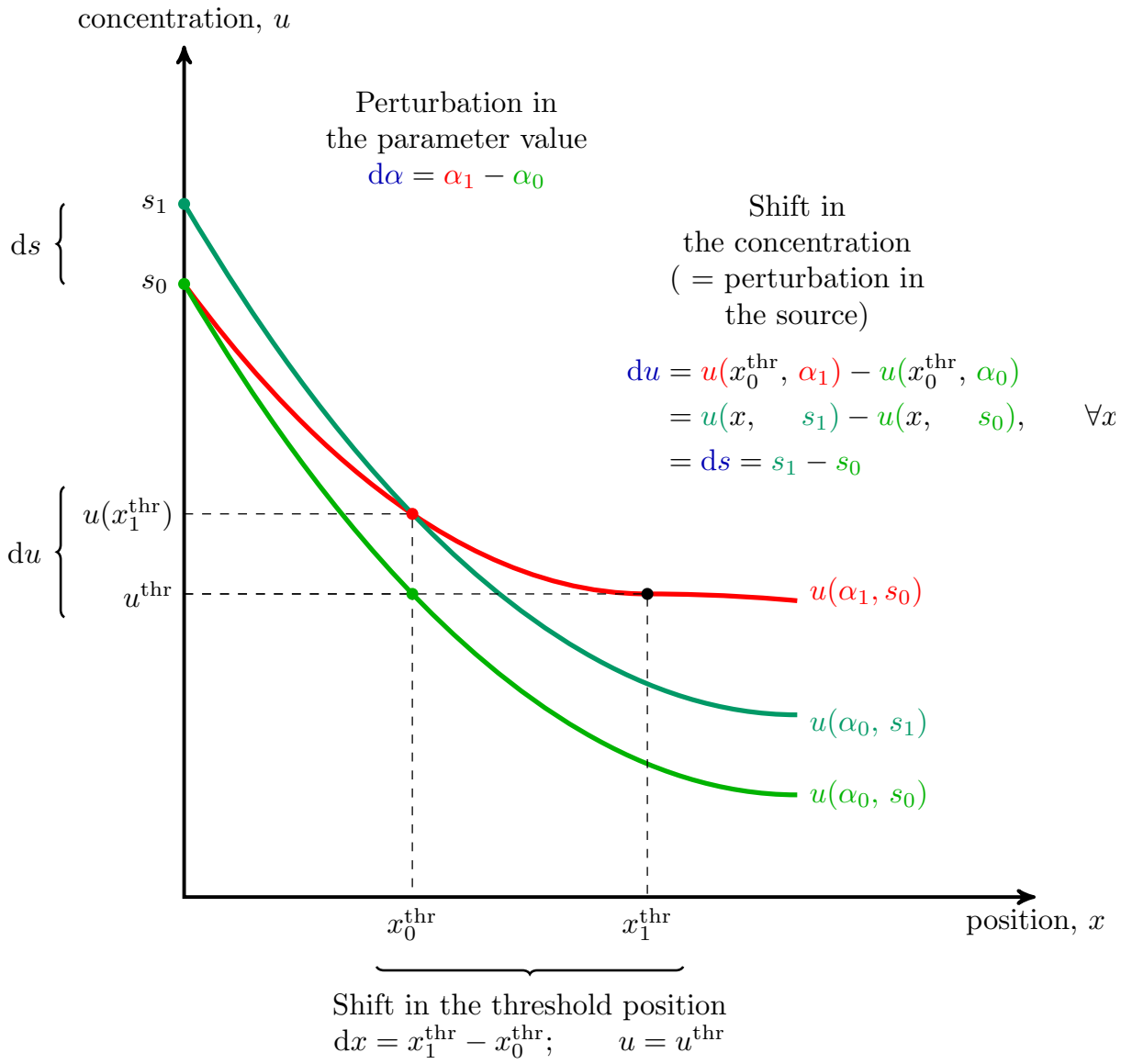

Fig. S9. The principle of the sensitivity analysis. The profile of the morphogen under physiological conditions is shown in green. We study the behavior of the threshold position (x_0^{thr}), defined by the threshold concentration (u^{thr}), upon perturbation in the parameter values. After perturbing parameter α by some small value $\mathrm{d}\alpha$, we obtain another, distorted profile (in red), where the threshold concentration (u^{thr}) is pointing to another x-position, x_1^{thr}. The concentration in the physiological threshold position is now shifted by $\mathrm{d}u$. Equivalently, the same value of concentration shift is achieved at all the x-positions if we perturb the source by $\mathrm{d}s = \mathrm{d}u$. The chain rule given in the supplementary text provides the connection between these shifts.

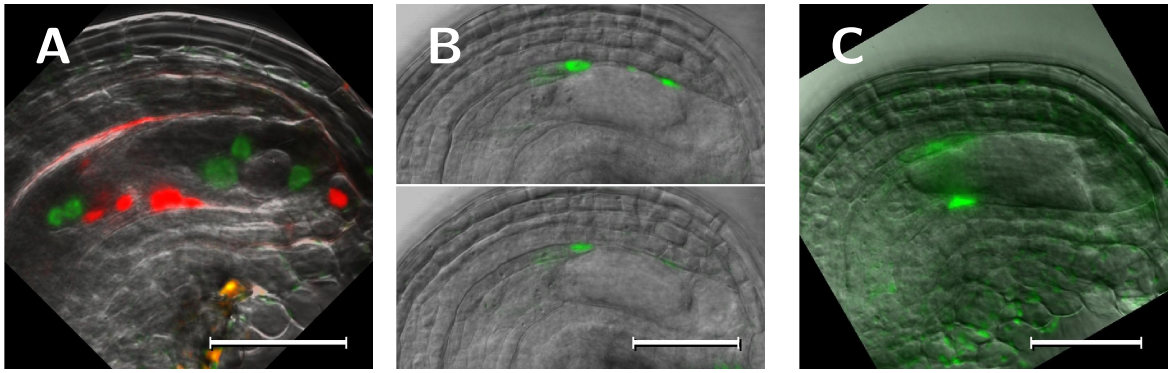

Fig. S10. *DR5* activity at the FG5 and FG6 stage in *Arabidopsis* ovules is observed only in the sporophytic tissue (**A**) At the FG5 stage, DR5::NLS:tdTomato expression in the ovule is localized to the nucellar cells on the lower (concave) side of the ovule along the whole length of the FG, with a stronger signal in the chalazal part; the gametic cell fate marker (green, AKV::H2B:YFP) shows no colocalization with the red DR5 signal. (**B**) Two z-sections of a FG at the FG5 stage are shown. DR5::SV40:3GFP is expressed in the endothelial cells adjacent to the chalazal pole of the FG. (**C**) DR5::GFP-ER expression in the FG5 stage: DR5 signal is observed in the endothelial cells surrounding the chalazal pole of the FG; the endothelial cells near the micropylar part have already degraded. Scale bars: 30 μm.

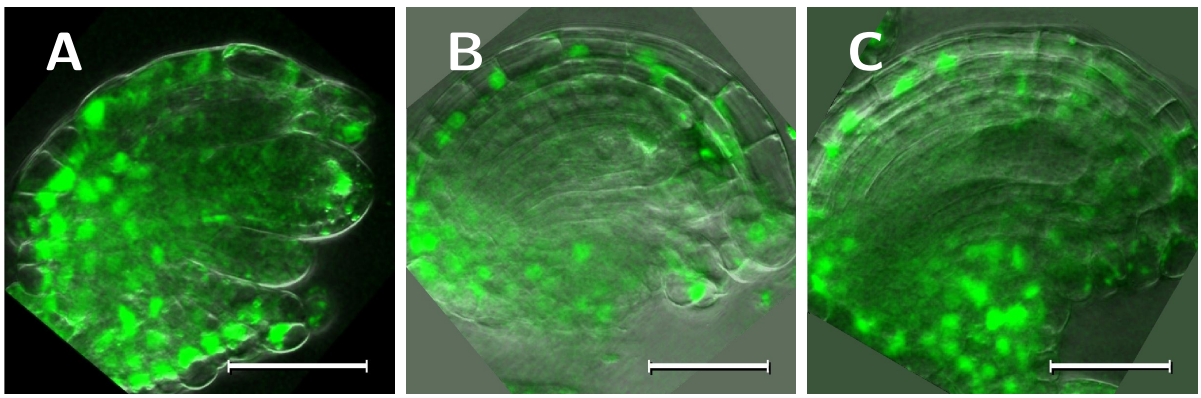

Fig. S11. The 35S::DII-Venus sensor is expressed in the outer integument and the chalazal pole but not in the female gametophyte of the *Arabidopsis* ovules. (**A**) Functional megaspore stage: the DII-Venus fluorescence is strong in the chalaza of the ovule and in a micropylar-most nucellar cells. (**B**) FG3 stage: the DII-Venus fluorescence appears in the outer integument. (**C**). FG4 stage. Note, at no stage can the DII-Venus fluorescence be seen within the FG. Scale bars: 30 μm.

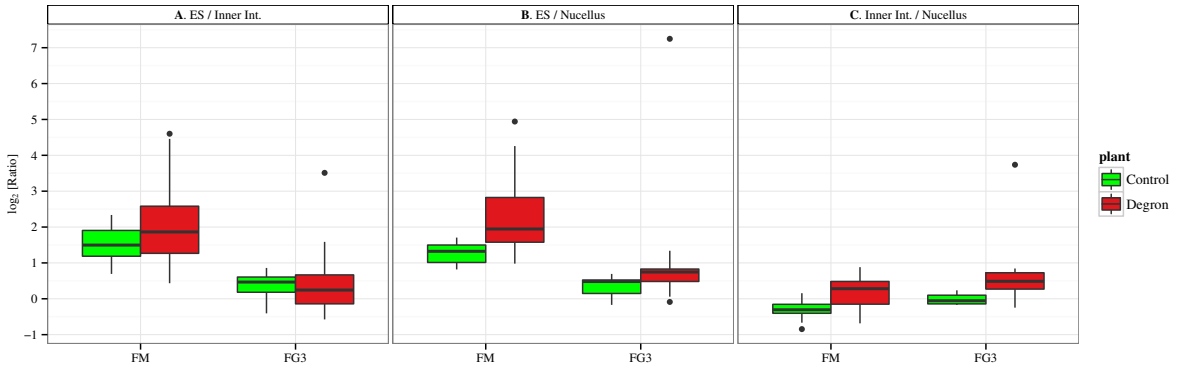

Fig. S12. Quantification of the fluorescence in the pUBQ10::degron:GFP and the pUBQ10::GFP plants indicates that the pattern of the auxin activity in the ovules is consistent with the *DR5* expression. Accounting for the non-uniform activity of the UBQ10 promoter driving the degron:GFP sensor construct, we performed intensity ratio measurements in the control pUBQ10::GFP and sensor pUBQ10::degron:GFP plants in order to infer the pattern of auxin distribution in the developing ovules. The GFP fluorescent images (grayscale, 12-bit) of the ovules from the degron (pUBQ10::degron:GFP) and the control (pUBQ10::GFP) transgenic lines were manually segmented and the median of the intensity was quantified using the ImageJ software. The intensity was measured for three regions (FG, endothelium surrounding the FG, and inner integument) from 2 degron lines and 6 control lines at stages the functional megaspore (FM) and late two-nucleate stage (FG3; all stages according to Christensen et al., 1997) ($n > 6$ per group). The $\log_2$-transformed ratios between the median intensity of the regions for each image were subjected to a one-sided Wilcoxon signed-rank test in R software (version 2.14.1). (**A**) The intensity ratio between the FG and the inner integument is insignificantly higher in the degron carrying plants at the FM stage and approximately the same at the FG3 stage, suggesting that the level of auxin is lower in the FG than in the inner integument at the FM stage and similar at the FG3 stage. (**B**) The intensity ratio between the FG and the nucellus is higher in the degron carrying plants at the functional megaspore (FM) stage (also referred to as FG1) and possibly lower at the FG3 stage, suggesting that the level of auxin is lower in the FG than in the nucellus at this stage and possibly lower at the FG3 stage. (**C**) In the degron plants, the fluorescence intensity ratio between the inner integument and the nucellus is significantly lower compared to the control at both FM and FG3 stage, which suggests that auxin activity in the inner integument is lower than in the nucellus. Significance levels: * –$p < 0.004$ (significant); † $p < 0.15$ (insignificant trend).

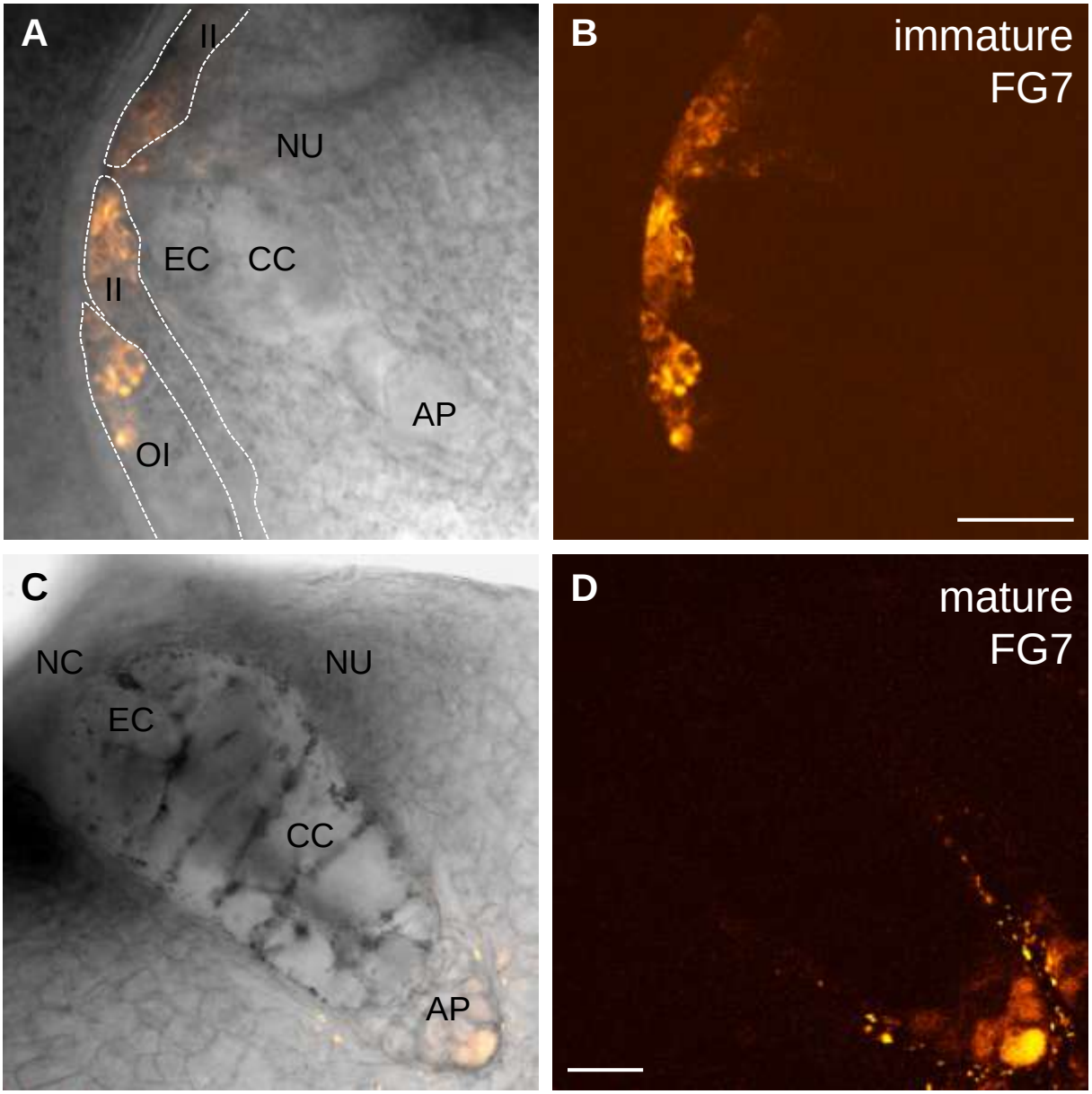

Fig. S13. Auxin response in the micropylar tips of integuments and at the chalazal pole inside the mature female gametophyte of maize. Auxin response is indirectly visualized by the activity of the synthetic *DR5* promoter driving ER localized mRFP marker protein expression. (**A**) Early FG at stage FG7. Antipodals start to proliferate. Strong mRFP signals signals are visible in the tips of the integuments (white dashed lines), but not in the micropylar nucellus cap. (**B**) Enhanced fluorescence image of (A) showing lack of mRFP signals inside the mature FG. (**C**) Mature FG. Integuments are removed. Strongest mRFP signal is visible in the antipodal cell most distant to the central cell. (**D**) Enhanced fluorescence image of (C) showing an mRFP gradient inside the antipodal cell cluster, with lowest signal in antipodal cells neighboring the central cell. (A and C) merged bright field and epifluorescent images. (B and D) Fluorescence images of (A) and (C), respectively. Abbreviations: AP: antipodal cells, CC: central cell, EC: egg cell, II: inner integument, NC: nucellar cap, NU: nucellus, OI: outer integument. Scale bars: 50 μm.

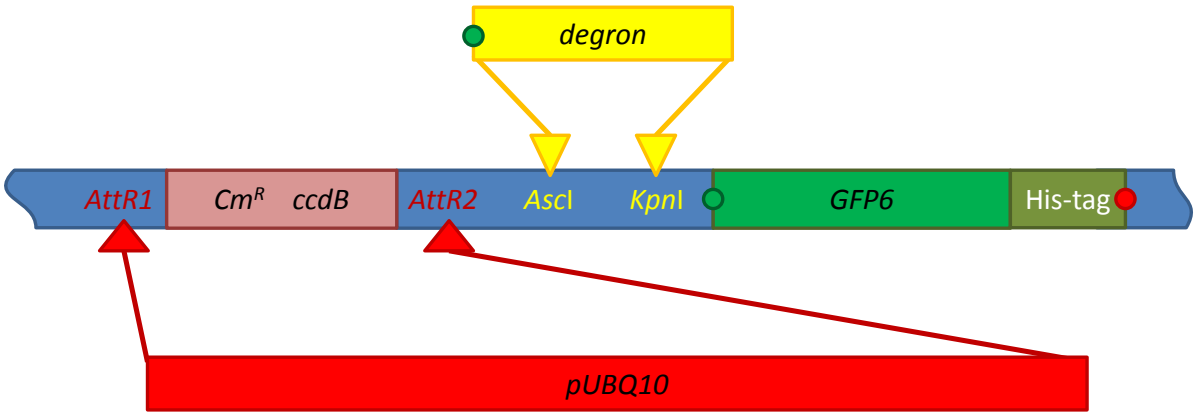

Fig. S14. Scheme of cloning of the pUBQ10::degron:GFP plasmid. The pUBQ10::degron:GFP plasmid was obtained in two steps. First, the pMDC111 (Curtis and Grossniklaus, 2003) destination vector was modified by inserting a sequence encoding the 6-amino acid long degron consensus core motif of domain II of AUX/IAA proteins, VGWPPV, between the AscI and KpnI restriction sites as a C-terminal in-frame fusion to GFP6-His-tag carried in the original vector. Subsequently, an entry clone carrying the 2.5 kb *Arabidopsis UBQ10* ubiquitin promoter was combined with the modified destination vector through a Gateway LR reaction.